Electronic Supplementary Material (ESI) for Inorganic Chemistry Frontiers.

Supporting Information

Exploiting the 'vacant' site in dinuclear $[Pd_2L_2]^{n+}$ metallo-cycles: multi-step control over binding affinity without alteration of core host structure

James Kolien,[a] Amanda R. Inglis,[a] Roan A. S. Vasdev,[b] Ben I. Howard,[a] Paul E. Kruger,[a] Dan Preston,[a,c]*

[a]MacDiarmid Institute for Advanced Materials and Nanotechnology, School of Physical and Chemical Sciences, University of Canterbury, Christchurch 8041, New Zealand.
[b]Department of Chemistry, University of Otago, PO Box 56, Dunedin 9054, New Zealand.
[c]Research School of Chemistry, The Australian National University, Canberra, ACT 2600, Australia.

***daniel.preston@anu.edu.au**

Contents

1 Contents

2 Experimental

2.1 General

Unless otherwise stated, all reagents were purchased from commercial sources and used without further purification, except for 1-(4-methylbenzenesulfonate)-2-[2-(2-methoxyethoxy)ethoxy]-ethanol,[1] 1-azido-3-bromo-benzene,[2] 4-(4-(4,4,5,5-tetramethyl-1,3,2-dioxaborolan-2-yl)phenyl)-pyridine,[3] and [((E-2-((2-oxidobenzylidene)amino)-phenolate)(DMSO)platinum(II)][4] which were synthesised according to literature procedure. Solvents were laboratory reagent grade. Abbreviations: methanol (MeOH), dichloromethane (DCM), ethylenediaminetetraacetate (EDTA), ethynyltrimethylsilane (TMS-acetylene), tetrahydrofuran (THF), dimethyl sulfoxide (DMSO), dimethylformamide (DMF). The 0.1 M EDTA solution used in work-up is made up of 7.5g EDTA, 225 mL distilled water and 25 mL ammonia solution. ^{1}H and ^{13}C NMR spectra were recorded on a JOEL 600 NMR spectrometer operating at 600 MHz for ^{1}H and 150 MHz for ^{13}C NMR. Chemical shifts are reported in parts per million and referenced to residual solvent peaks ($CDCl_3$: ^{1}H δ 7.26 ppm, ^{13}C δ 77.16 ppm; d_6-DMSO: ^{1}H δ 2.50 ppm; CD_3CN: ^{1}H δ 1.94 ppm). Coupling constants (J) are reported in Hertz (Hz). Standard abbreviations indicating multiplicity were used as follows: m = multiplet, t = triplet, d = doublet, dd = double doublet, s = singlet. Infrared measurements were carried out using a Bruker ALPHA Platinum ATR FT-IR spectrometer measuring in the range 4000-450 cm^{-1}. High-resolution mass spectra (HRMS) were collected on a Bruker maXis 4G time of flight spectrometer operating in ESMS+ mode. **CAUTION:** Azides are explosive and toxic and care should be taken when handling them. Reactions were carried out on small scale. No problems were encountered during the course of this work.

NOTE: In the mass spectral analysis, the term 'M' refers to $[Pd_2L_2](BF_4)_4$ for the tetracationic complex or $[Pd_2L_2L'_2](BF_4)_2$ from the dicationic complexes.

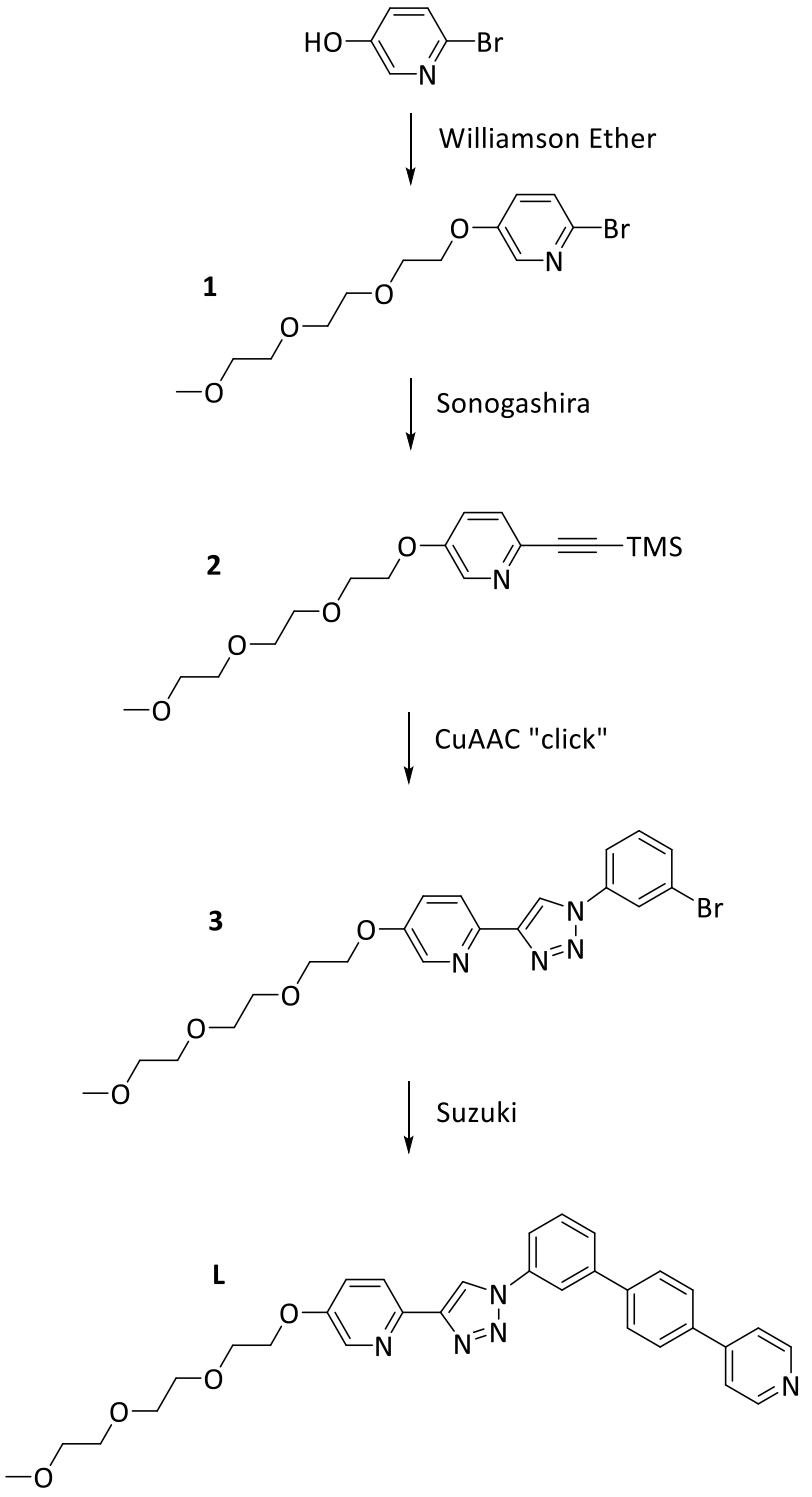

Figure 2.1 General synthetic strategy to obtain ligand **L**.

2.2 Synthesis of 1

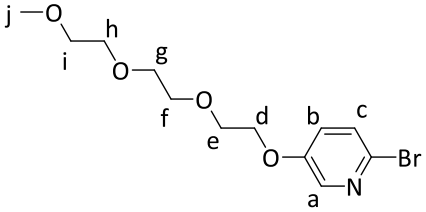

The combination of 1-(4-methylebenzenesulfonate)-2-(2-(2-methoxyethoxy)ethoxy)ethanol[1] (1.50 g, 4.71 mmol), 2-bromo-5-hydroxypyridine (0.547 g, 3.14 mmol), and K_2CO_3 (0.868 g, 6.28 mmol) in DMF (40 mL) was stirred overnight at 100 °C. After filtration through cotton wool, the solvent was removed under vacuum. The residue was then dissolved in DCM, washed with water (5 x 100 mL), and the solvent removed under vacuum. Purification through column chromatography on silica (DCM to 4:1 DCM/acetone) gave the product as a light yellow oil (0.800 g, 2.50 mmol, 80%). ^{1}H NMR (600 MHz, $CDCl_3$, 298 K) δ: 8.07 (1H, d, J = 3.0 Hz, H_a), 7.36 (1H, d, J = 8.6 Hz, H_c), 7.14 (1H, dd, J = 8.6, 3.1 Hz, H_b), 4.16-4.14 (2H, m, H_d), 3.87-3.85 (2H, m, H_e), 3.73-3.72 (2H, m, H_f), 3.68-3.66 (2H, m, H_g), 3.65-3.63 (2H, m, H_h), 3.55-3.53 (2H, m, H_i), 3.37 (3H, s, H_j). ^{13}C NMR (150 MHz, $CDCl_3$, 298 K) δ: 154.9, 137.6, 132.3, 128.3, 125.3, 72.0, 71.0, 70.8, 70.7, 69.6, 68.4, 59.2. HR ESI-MS (DCM/MeOH) m/z = 320.0527 $[MH]^+$ (calc. for $C_{12}H_{18}BrNO_4$, 320.0492). IR (cm^{-1}) 2874, 1448, 1366, 1270, 1226, 1090, 1053, 922, 829.

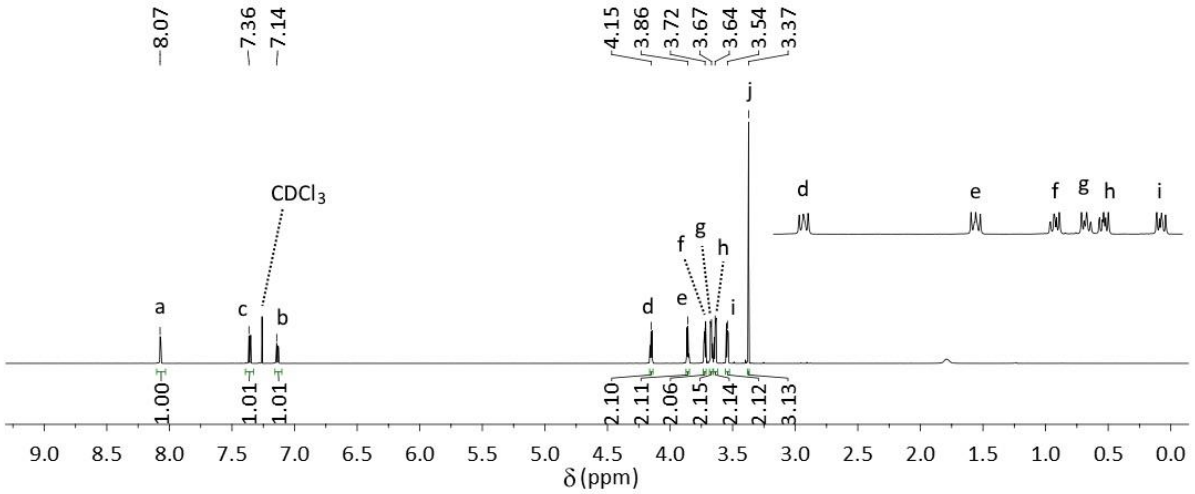

Figure 2.2 ^{1}H NMR spectrum (600 MHz, $CDCl_3$, 298 K) of **1**.

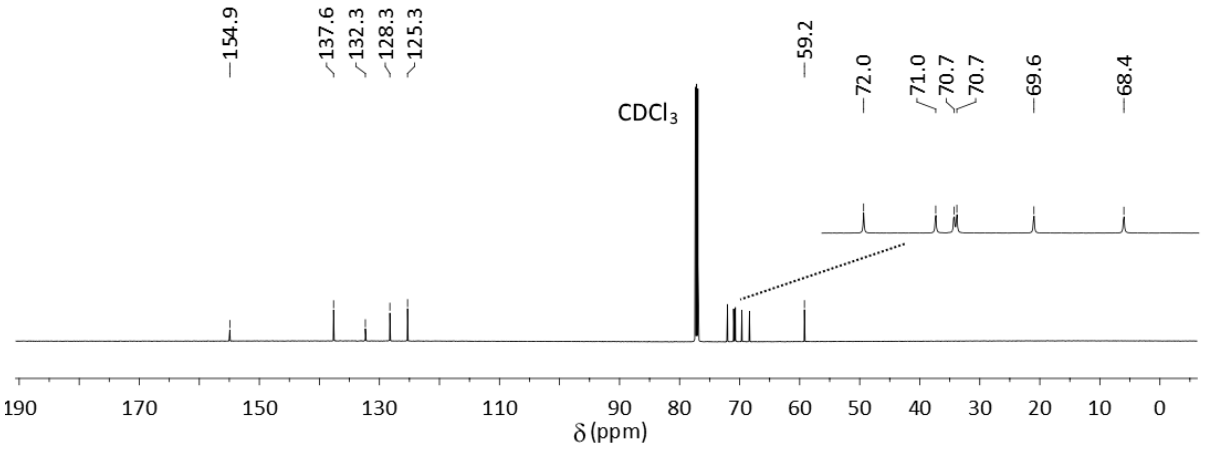

Figure 2.3 ^{13}C NMR spectrum (150 MHz, $CDCl_3$, 298 K) of **1**.

2.3 Synthesis of 2

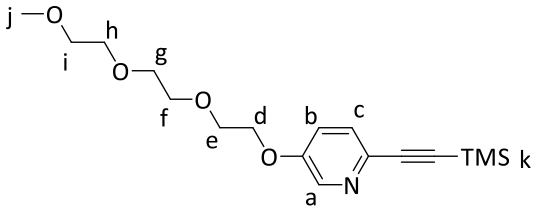

A sealed tube with **1** (1.01 g, 3.15 mmol) in diisopropylamine (3 mL) was degassed with nitrogen for 10 minutes. Copper iodide (0.061 g, 0.32 mmol), ethynyltrimethylsilane (0.460 g, 4.68 mmol) and $[Pd(PPh_3)_2Cl_2]$ (0.118 g, 0.168 mmol) was then added, and the reaction stirred overnight in a sealed tube at 90 °C. After addition of DCM (100 mL) and aqueous 0.1 M EDTA/NH_4OH (100 mL) and stirring for 30 minutes, the organic layer was washed with water (4 x 100 mL), and the solvent removed under vacuum. Purification through column chromatography on silica (DCM to 10:1 DCM/acetone) gave the product as a dark brown oil (0.889 g, 2.63 mmol, 83%). ^{1}H NMR (600 MHz, $CDCl_3$, 298 K) δ: 8.26 (1H, d, J = 2.9 Hz, H_a), 7.39 (1H, d, J = 8.6 Hz, H_c), 7.16 (1H, dd, J = 8.8, 2.9 Hz, H_b), 4.18-4.17 (2H, m, H_d), 3.87-3.86 (2H, m, H_e), 3.74-3.72 (2H, m, H_f), 3.68-3.66 (2H, m, H_g), 3.65-3.63 (2H, m, H_h), 3.55-3.53 (2H, m, H_i), 3.37 (3H, s, H_j), 0.25 (9H, s, H_k). ^{13}C NMR (150 MHz, $CDCl_3$, 298 K) δ: 154.6, 138.5, 135.3, 128.0, 121.2, 103.5, 93.4, 72.0, 71.0, 70.8, 70.7, 69.6, 68.1, 59.2, -0.1. HR ESI-MS (DCM/MeOH) *m/z* = 338.1826 $[MH]^+$ (calc. for $C_{17}H_{28}NO_4Si$, 338.1782). IR (cm^{-1}) 2955, 2876, 2162, 1565, 1467, 1249, 1105, 1054, 866, 838, 759.

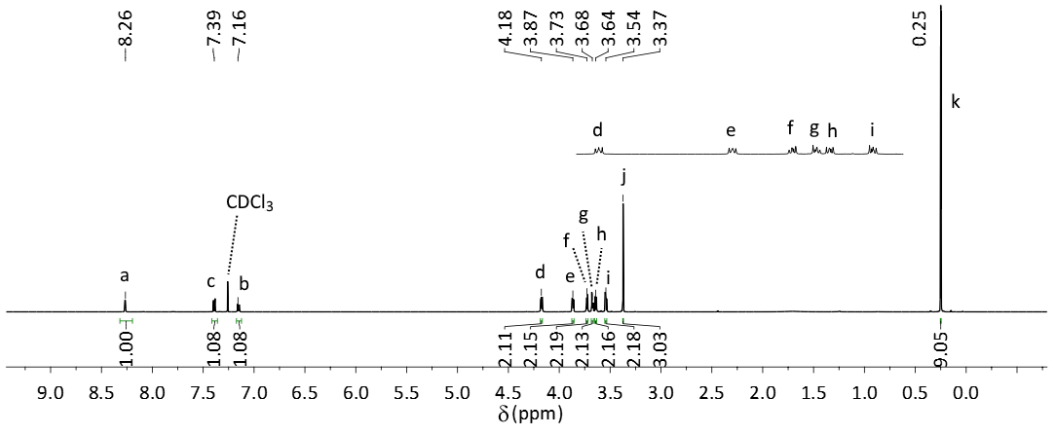

Figure 2.4 ^{1}H NMR spectrum (600 MHz, $CDCl_3$, 298 K) of **2**.

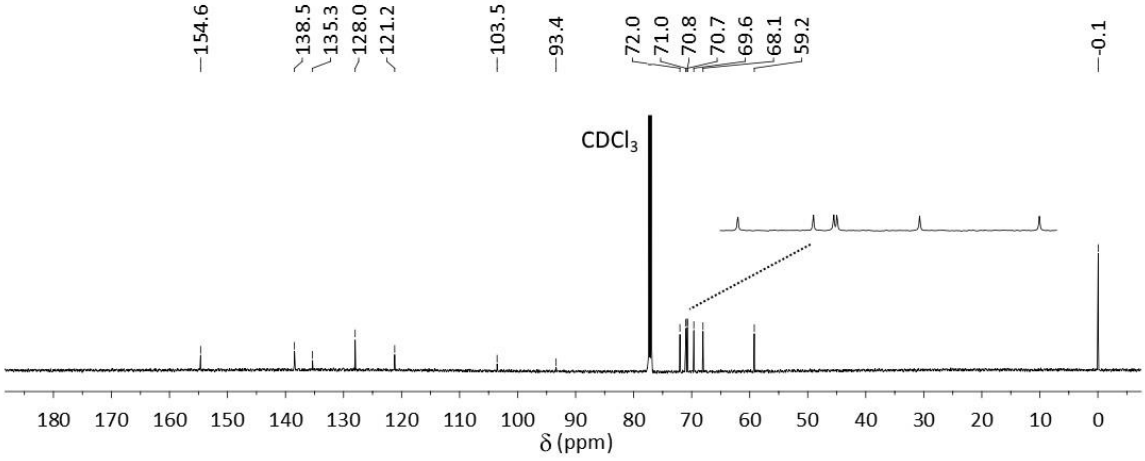

Figure 2.5 ^{13}C NMR spectrum (150 MHz, $CDCl_3$, 298 K) of **2**.

2.4 Synthesis of 3

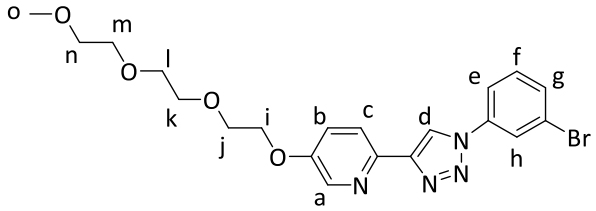

A mixture of **2** (0.457 g, 1.90 mmol) and Na_2CO_3 (0.402 g, 3.79 mmol) were stirred in DMF (10 mL) for 5 minutes. 1-azido-3-bromo-benzene (made and used immediately without purification as per literature method,[2] 0.455 g, 2.30 mmol), L-ascorbic acid (0.334 g, 1.90 mmol), $CuSO_4.5H_2O$ (0.152 g, 0.609 mmol), DMF (10 mL) and water (6 mL) was added. This solution was stirred overnight at room temperature. 100 mL of EDTA solution and 100 mL DCM was added to the solution and stirred for 30 minutes. The organic layer was washed with water (4 x 100 mL), and the solvent removed under vacuum. Purification through column chromatography on silica (DCM to 5:1 DCM/acetone) gave the product as a light orange solid (0.540 g, 1.17 mmol, 61%). ^{1}H NMR (600 MHz, $CDCl_3$, 298 K) δ: 8.52 (1H, s, H_d), 8.33 (1H, d, J = 2.8 Hz, H_a), 8.16 (1H, d, J = 8.7 Hz, H_c), 8.03 (1H, t, J = 2.0 Hz, H_h), 7.75 (1H, m, H_e), 7.58 (1H, dd, J = 8.5, 2.1 Hz, H_g), 7.42 (1H, t, J = 8.0 Hz, H_f), 7.36 (1H, dd, J = 8.6, 2.6 Hz, H_b), 4.24-4.23 (2H, m, H_i), 3.92-3.90 (2H, m, H_j), 3.77-3.75 (2H, m, H_k), 3.71-3.69 (2H, m, H_l), 3.67-3.65 (2H, m, H_m), 3.57-3.55 (2H, m, H_n), 3.38 (3H, s, H_o). ^{13}C NMR (150 MHz, CD_3CN, 298 K) δ: 155.0, 148.8, 142.3, 138.0, 137.6, 131.9, 131.3, 123.7, 123.5, 122.4, 121,3, 119.3, 118.9, 72.0, 71.0, 70.8, 70.7, 69.7, 68.2, 59.2. HR ESI-MS (DCM/MeOH) m/z = 463.1010 $[MH]^+$ (calc. for $C_{20}H_{23}BrN_4O_4$, 463.0975). IR (cm^{-1}) 2971, 2885, 2809, 1590, 1482, 1359, 1266, 1115, 1062, 1029, 926, 872, 850, 796, 778, 748.

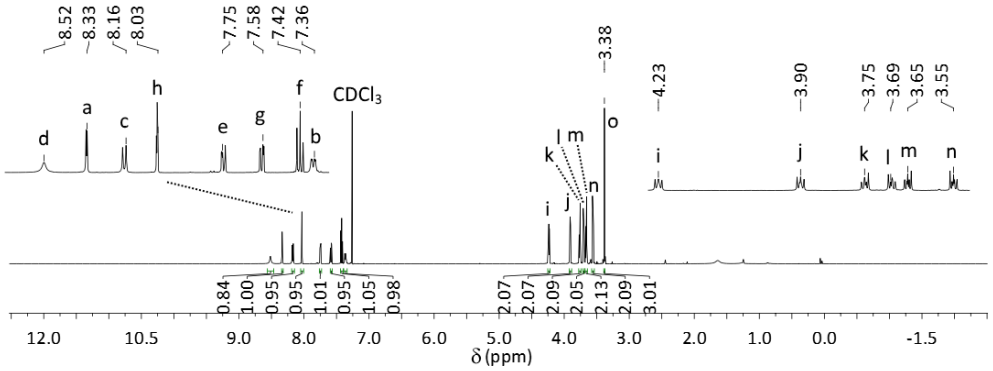

Figure 2.6 ^{1}H NMR spectrum (600 MHz, $CDCl_3$, 298 K) of **3**.

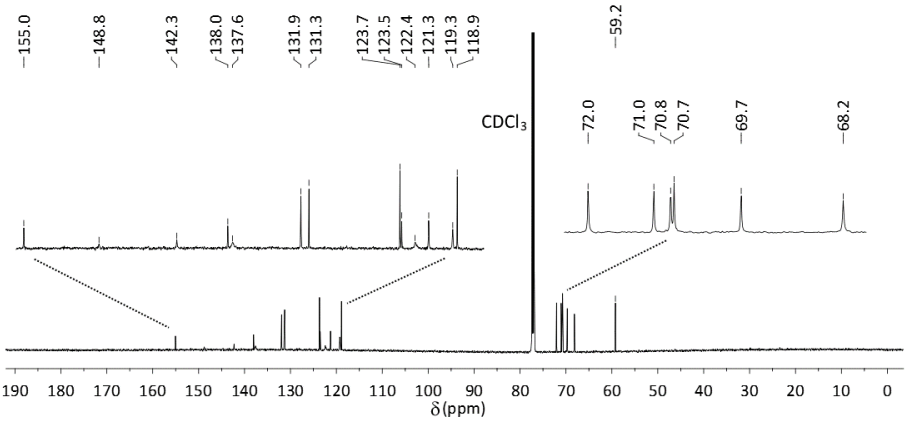

Figure 2.7 ^{13}C NMR spectrum (150 MHz, $CDCl_3$, 298 K) of **3**.

2.5 Synthesis of L

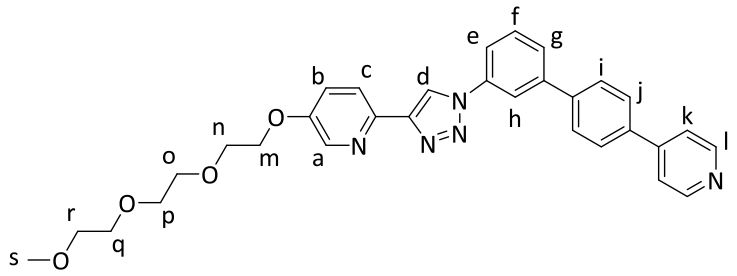

A 2:1 mixture of DMF/water (15 mL) was degassed with nitrogen for 2 hours. Against a positive nitrogen flow, **3** (0.300 g, 0.647 mmol), 4-(4-(4,4,5,5-tetramethyl-1,3,2-dioxaborolan-2-yl)phenyl)-pyridine,[3] 0.237 g, 0.842 mmol), Na_2CO_3 (0.532 g, 5.02 mmol), [$Pd_2(dba)_3$] (0.030 g, 0.032 mmol) and [$HP(tBu)_3$](BF_4) (0.038 g, 0.13 mmol) were added. The system was purged with nitrogen for an additional hour. The reaction was then stirred overnight at 140 °C under a nitrogen atmosphere. After addition of DCM (100 mL) and water (100 mL), the organic layer was washed with water (5 x 100 mL) and brine (100 mL). The solvent was then removed under vacuum. Silica column chromatography (using DCM to 1:1 DCM/acetone) gave the product as an off-white solid (0.308 g, 0.574 mmol, 89%). ^{1}H NMR (600 MHz, $CDCl_3$, 298 K) δ: 8.72 (2H, d, J = 6.1 Hz, H_l), 8.64 (1H, s, H_d), 8.35 (1H, d, J = 2.8 Hz, H_a), 8.22 (1H, d, J = 8.7 Hz, H_c), 8.13 (1H, t, J = 1.48, H_h), 7.83-7.79 (5H, m, $H_{e,i,j}$), 7.74 (1H, d, J = 7.8 Hz, H_g), 7.69 (2H, d, J = 5.9 Hz, H_k), 7.66 (1H, t, J = 7.9 Hz, H_f), 7.39 (1H, dd, J = 8.8, 2.8 Hz, H_b), 4.26-4.24 (2H, m, H_m), 3.93-3.91 (2H, m, H_n), 3.78-3.76 (2H, m, H_o), 3.71-3.70 (2H, m, H_p), 3.69-3.67 (2H, m, H_q), 3.57-3.56 (2H, m, H_r), 3.39 (3H, s, H_s). ^{13}C NMR (150 MHz, $CDCl_3$, 298 K) δ: 154.9, 150.1, 149.0, 148.1, 142.7, 142.2, 140.6, 138.0, 137.8, 137.7, 130.5, 128.1, 127.8, 127.4, 121.9, 121.8, 121.1, 119.5, 119.2, 119.2, 72.0, 71.0, 70.8, 70.7, 69.7, 68.1, 59.2. HR ESI-MS (DCM/MeOH) m/z = 538.2466 $[MH]^+$ (calc. for $C_{31}H_{31}N_5O_4$, 538.2449). IR (cm^{-1}) 2873, 1593, 1577, 1477, 1394, 1267, 1236, 1096, 1056, 1027, 922, 812, 787, 737.

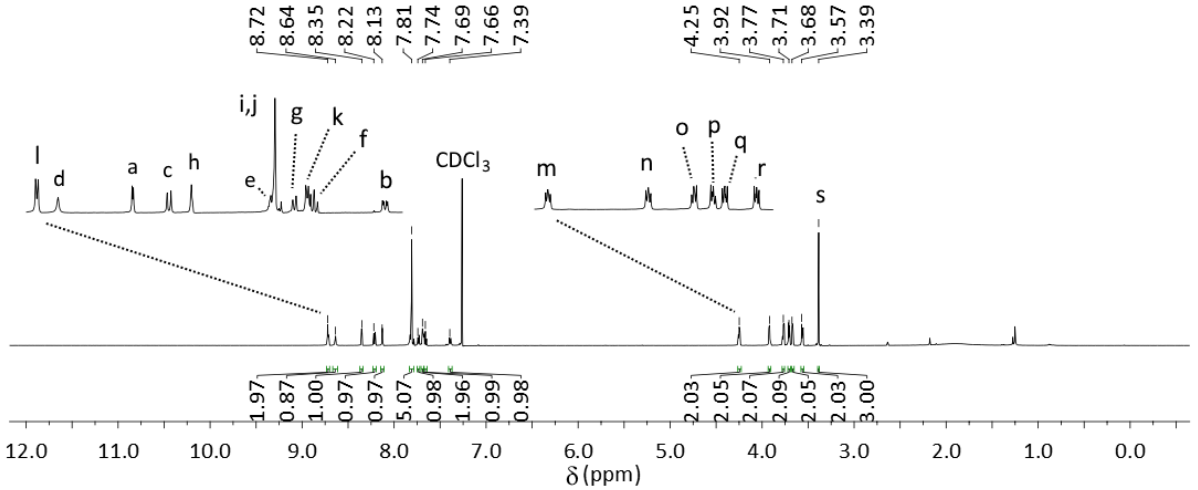

Figure 2.8 ^{1}H NMR spectrum (600 MHz, $CDCl_3$, 298 K) of **L**.

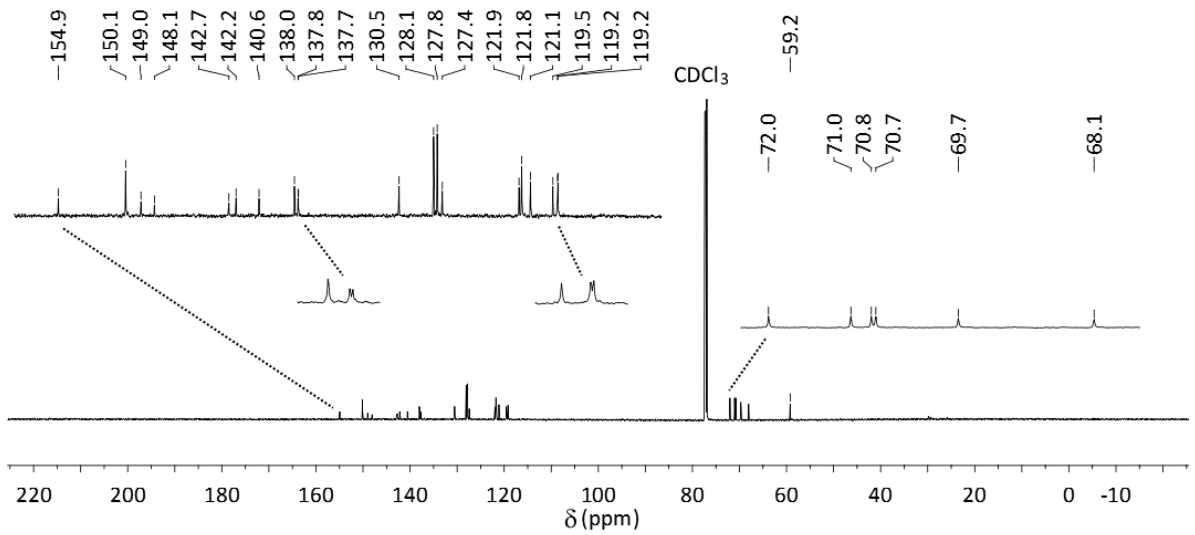

Figure 2.9 ^{13}C NMR spectrum (150 MHz, $CDCl_3$, 298 K) of **L**.

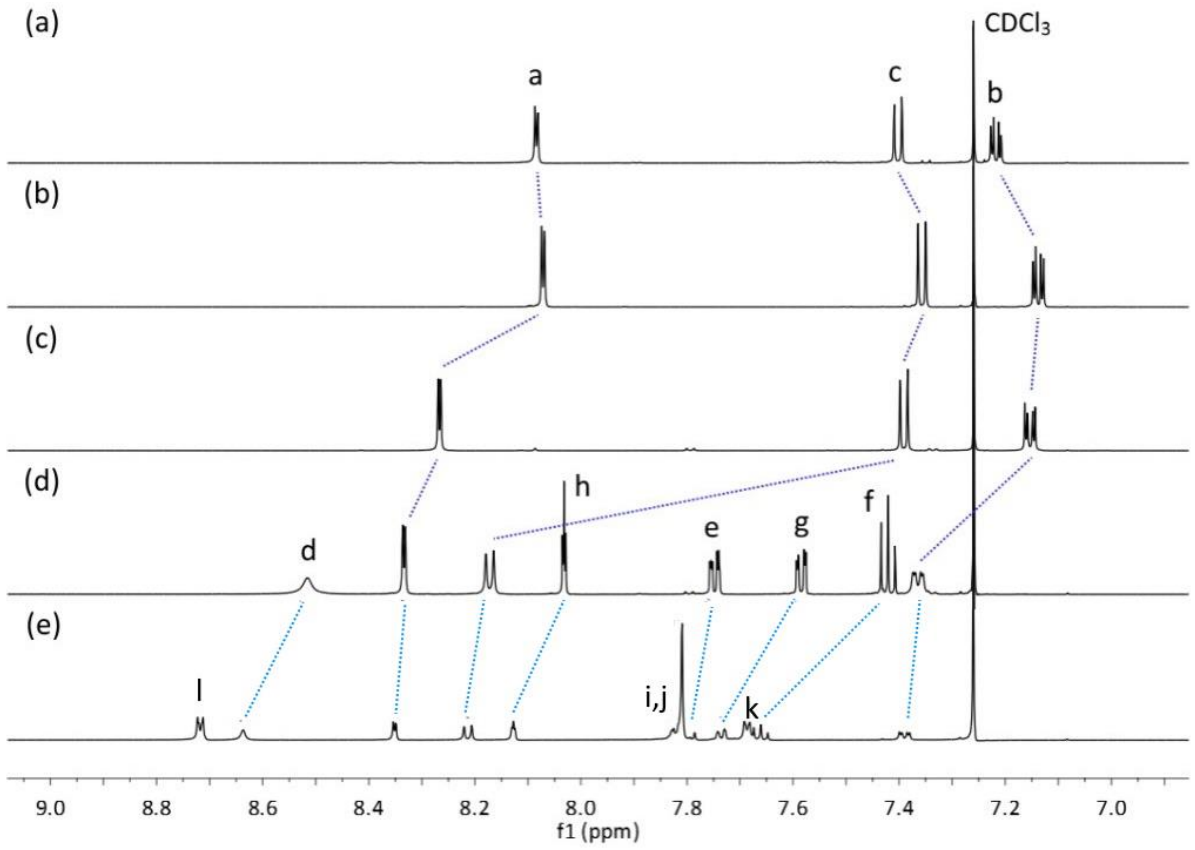

Figure 2.10 Partial stacked ^{1}H NMR spectra (600MHz, $CDCl_3$, 298 K) of the precursor molecules (2-bromo-5-hydroxypyridine (a), **1** (b), **2** (c), and **3** (d)), and **L** (e).

2.6 Synthesis of 2Pt

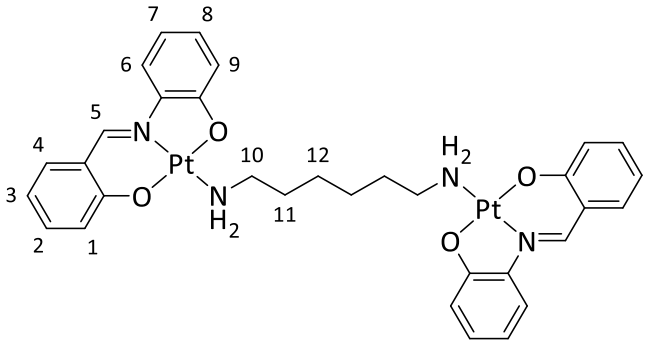

A combination of [((E-2-((2-oxidobenzylidene)amino)-phenolate)(DMSO)platinum(II)][4] (**Pt**) (120 mg, 24.8 mmol) in acetonitrile (6 mL) under a N_2 atmosphere had a solution of 1,6-diaminohexane (14 mg, 12 mmol) in acetonitrile (1 mL) added. The reaction was heated under N_2 at reflux for 16 hours. After cooling to room temperature, the solid was collected via filtration, and washed with acetonitrile (1 mL) to give the product as an orange solid (101 mg, 11.0 mmol, 89%). ^{1}H NMR (600 MHz, [D_6]DMSO, 298 K) δ: 9.26 (2H, s, H_5), 8.09 (2H, d, J = 8.4 Hz, H_4), 7.86 (2H, d, J = 8.0 Hz, H_6), 7.43 (2H, t, J = 8.6 Hz, H_8), 7.05 (2H, d, J = 8.5 Hz, H_9), 7.00 (2H, t, J = 6.9 Hz, H_2), 6.93 (2H, d, J = 8.3 Hz, H_1), 6.74 (2H, t, J = 7.9 Hz, H_7), 6.62 (2H, t, J = 8.3 Hz, H_3), 5.56 (4H, t, J = 6.6 Hz, NH_2), 2.81 (4H, quin, J = 7.7 Hz, H_{10}), 1.75 (4H, quin, J = 7.9 Hz, H_{11}), 1.37 (4H, quin, J = 6.9 Hz, H_{12}). ^{13}C NMR (125 MHz, [D_6]DMSO, 298 K) δ: 168.1, 161.0, 143.2, 139.8, 134.2, 132.1, 128.1, 122.5, 121.1, 117.4, 116.0, 115.8, 114.6, 45.1, 30.1, 26.3. HR ESI-MS (DMSO/DCM) m/z = 929.1943 $[M]^+$ (calc. for $C_{32}H_{34}N_4O_4Pt_2$, 929.1938). IR ν (cm^{-1}) 3347 3216 3067 2926 2856 1640 1596 1580 1475 1434 1307 1215 1168 1150 1030 741.

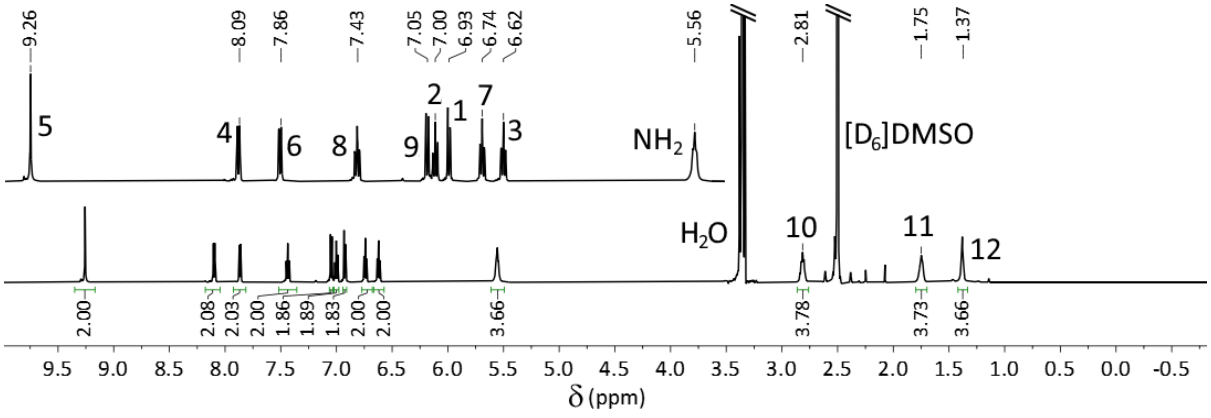

Figure 2.11 ^{1}H NMR spectrum (600 MHz, [D_6]DMSO, 298 K) of **2Pt**.

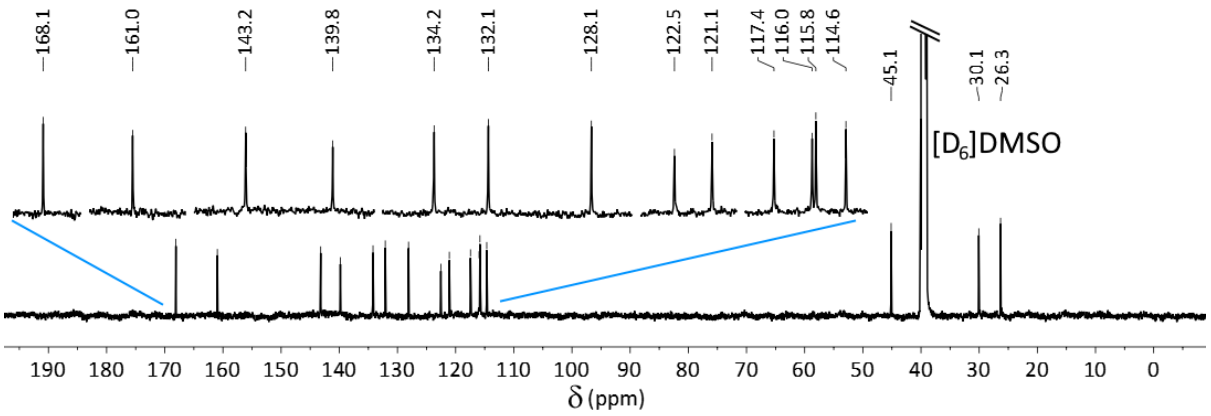

Figure 2.12 ^{13}C NMR spectrum (125 MHz, [D_6]DMSO, 298 K) of **2Pt**.

2.7 Synthesis of $[Pd_2L_2(solvent)_2](BF_4)_4$

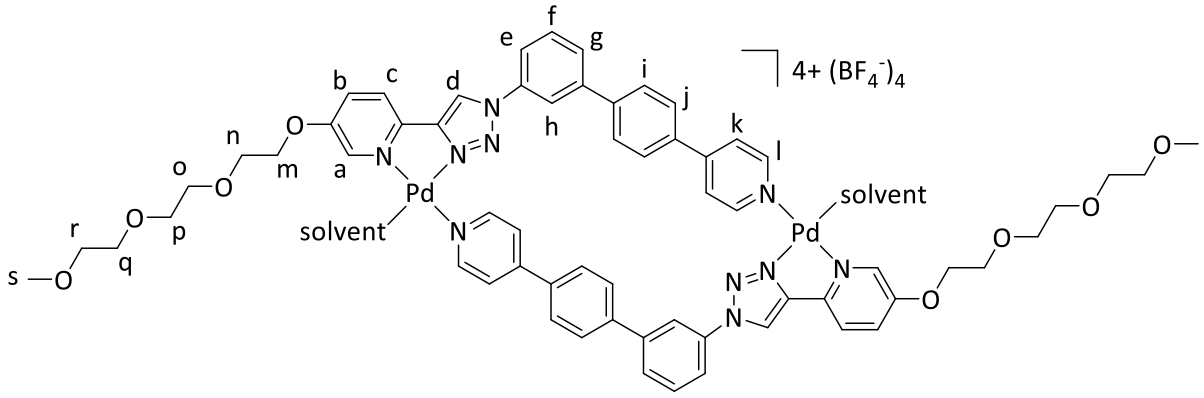

A solution of **L** (3.6 mg, 6.7 µmol) in CD_3CN (0.5 mL) was combined with a solution of $[Pd(CH_3CN)_4](BF_4)_2$ (3.0 mg, 6.8 µmol) in CD_3CN (0.1 mL), giving a total volume of 0.6 mL. Solutions generated in DMSO yielded similar results. Vapour diffusion of diethyl ether gave a tan precipitate (5.0 mg, 2.9 µmol, 87%). ^{1}H NMR (600 MHz, CD_3CN, 298 K) *integration given per ligand δ*: 9.23 (1H, s, H_d), 8.89 (2H, d, *J* = 6.5 Hz, H_l), 8.30 (1H, s, H_a), 8.17 (1H, t, *J* = 1.9 Hz, H_h), 8.16 (1H, d, *J* = 8.9 Hz, H_c), 8.11 (2H, d, *J* = 6.8 Hz, H_k), 7.99-7.97 (4H, m, $H_{b,g,j}$), 7.91 (2H, d, *J* = 8.3 Hz, H_i), 7.84 (1H, dd, *J* = 8.2, 1.7 Hz, H_e), 7.78 (1H, t, *J* = 7.9 Hz, H_f), 4.42-4.40 (2H, m, H_m), 3.87-3.86 (2H, m, H_n), 3.65-3.63 (2H, m, H_o), 3.58-3.56 (2H, m, H_p), 3.56-3.54 (2H, m, H_q), 3.47-3.45 (2H, m, H_r), 3.27 (3H, s, H_s). The low concentration precluded the collection of a ^{13}C NMR spectrum. HR ESI-MS (DMSO/DMF) *m/z* = 444.4970 $[M - (BF_4^-)_4 + HCOO^-]^{3+}$ (calc. for $C_{63}H_{63}N_{10}O_{10}Pd_2$, 444.4270, *m/z* = 689.2482 $[M - (BF_4^-)_4 + (HCOO^-)_2]^{2+}$ (calc. for $C_{64}H_{64}N_{10}O_{12}Pd_2$, 689.1397), *m/z* = 947.6688 $[2M - (BF_4^-)_3 + (HCOO^-)_4]^-$ (calc. for $C_{126}H_{126}BF_4N_{10}O_{24}Pd_2$, 947.5213). IR ($cm^{-1}$) 3117, 2889, 1616, 1591, 1571, 1482, 1467, 1288, 1262, 1242, 1054, 1027, 821, 791, 756.

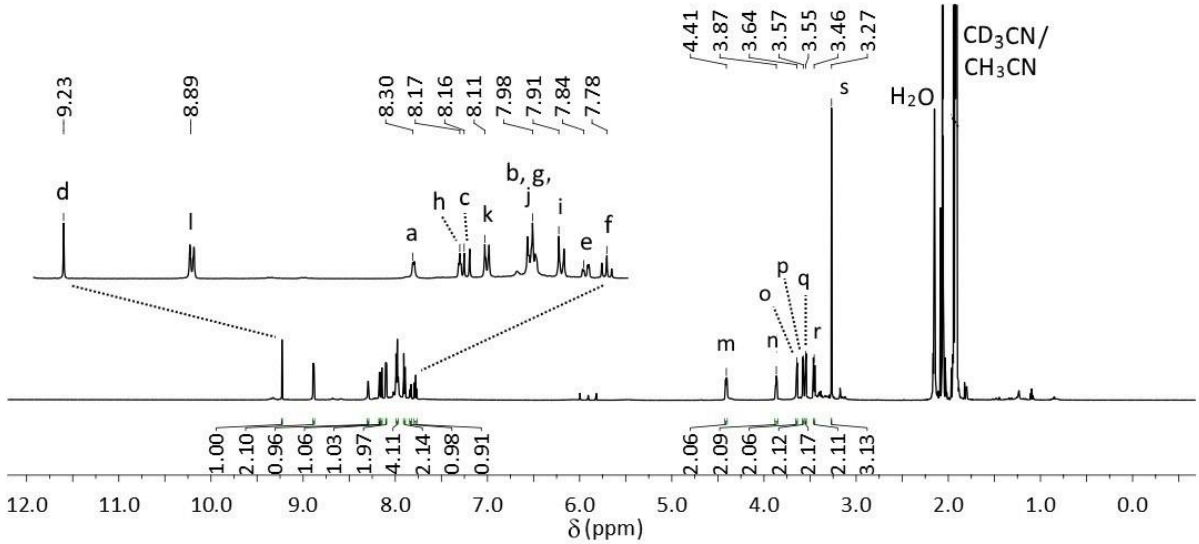

Figure 2.13 ^{1}H NMR spectrum (600 MHz, CD_3CN, 298 K) of $[Pd_2\mathbf{L}_2(CD_3CN)_2](BF_4)_4$.

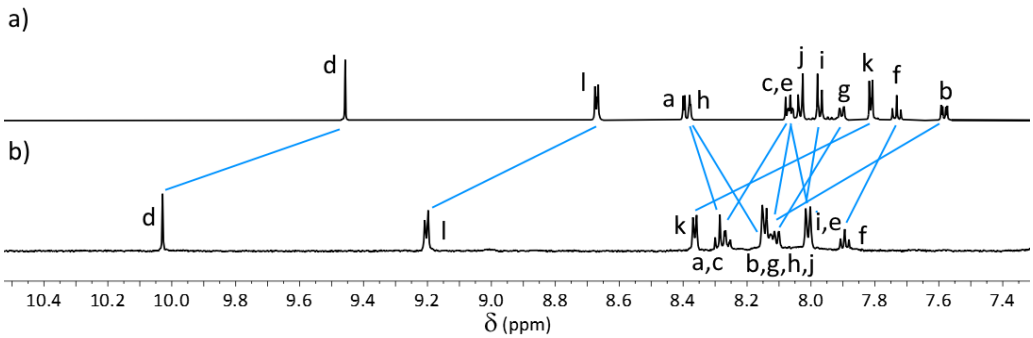

Figure 2.14 Partial stacked ^{1}H NMR spectra (600 MHz, [D$_6$]DMSO, 298 K) of a) **L**, and b) [Pd$_2$**L**$_2$(DMSO)$_2$](BF$_4$)$_4$.

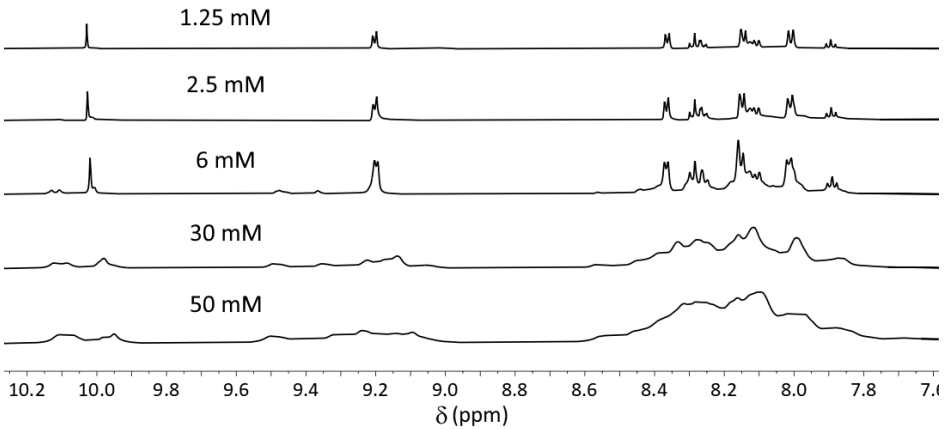

Figure 2.15 Partial stacked ^{1}H NMR spectra (600 MHz, [D$_6$]DMSO, 298 K) of [Pd$_2$**L**$_2$(DMSO)$_2$](BF$_4$)$_4$ at different concentrations

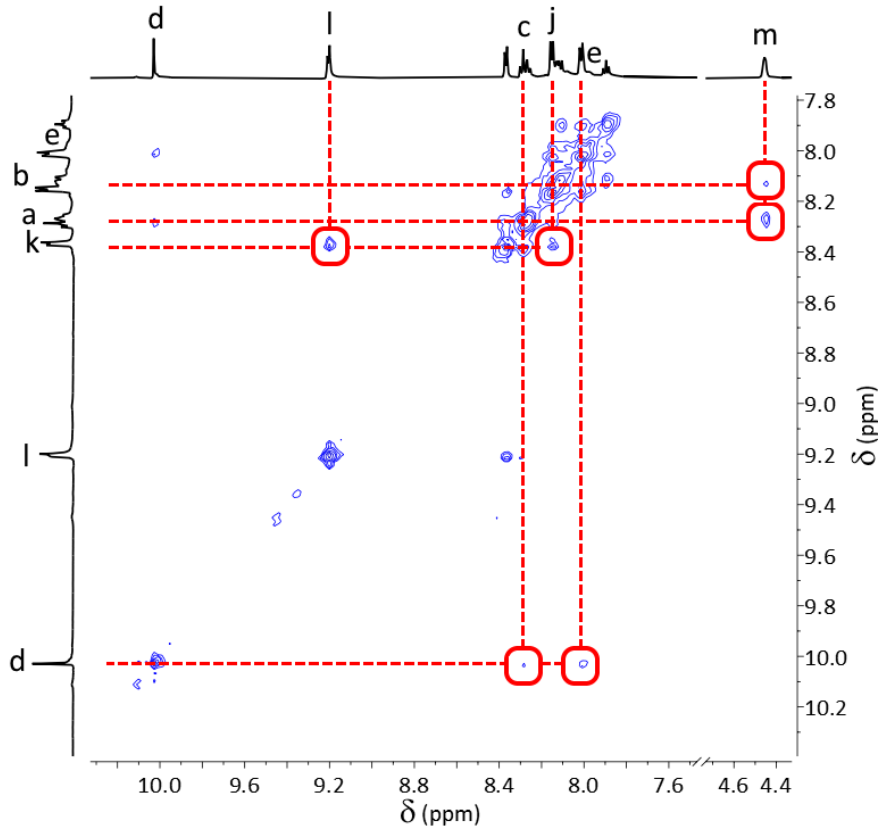

Figure 2.16 Partial ^{1}H 2D NMR NOESY spectrum (600 MHz, [D$_6$]DMSO, 298 K, 300 ms mixing time) of [Pd$_2$**L**$_2$(DMSO)$_2$]$^{4+}$.

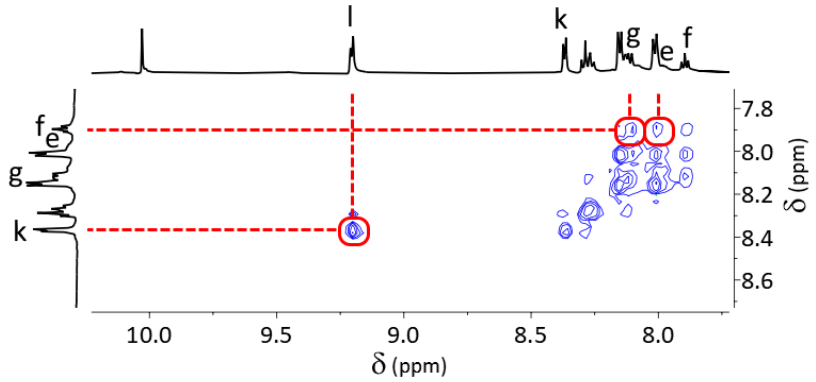

Figure 2.17 Partial ^{1}H NMR TOCSY spectrum (600 MHz, [D$_6$]DMSO, 298 K) of $[Pd_2\mathbf{L}_2(DMSO)_2]^{4+}$.

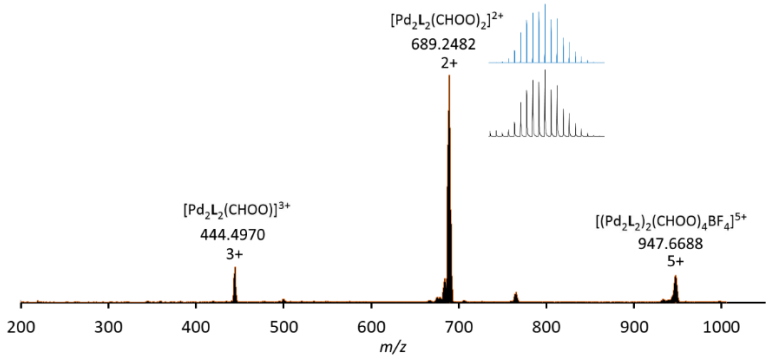

Figure 2.18 Mass spectrum (DMSO/DMF) of $[Pd_2\mathbf{L}_2(DMSO)_2](BF_4)_4$. We attribute the 947.6688 peak to association of two complexes in mass spectral conditions: the NMR sample from which this data was obtained showed only a single set of peaks. Formate generated *in situ* from the presence of formic acid under mass spectral conditions.

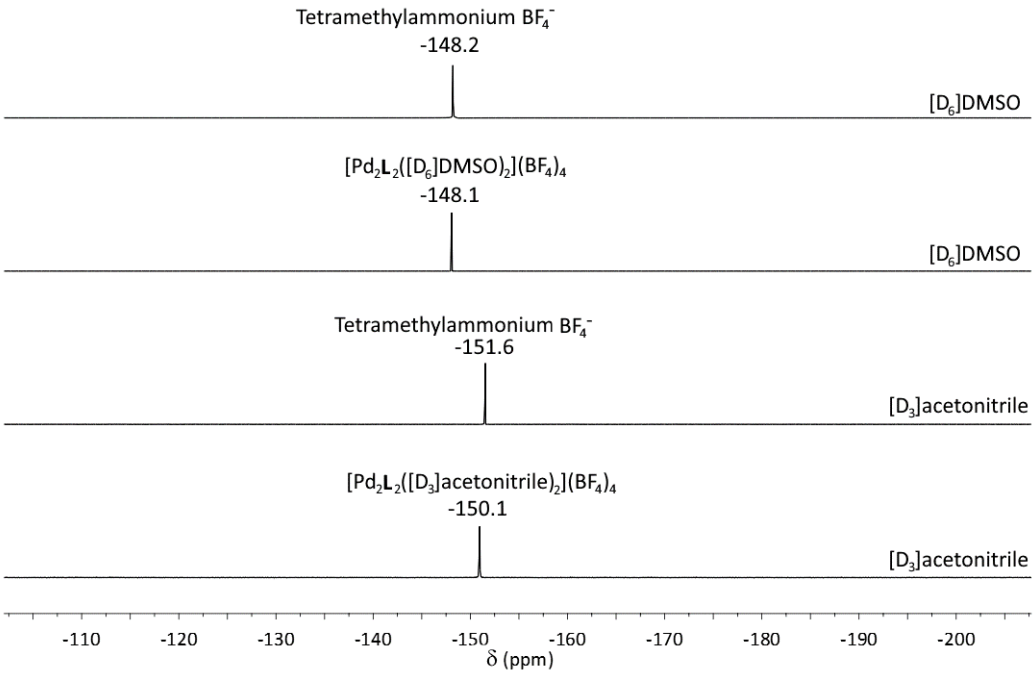

Figure 2.19 Partial stacked ^{19}F NMR spectra (376 MHz, 298K) in [D$_6$]DMSO or [D$_3$]acetonitrile, showing that the BF_4^- counterion is non-coordinating.

2.8 Synthesis of $[Pd_2(L2)_2(Cl)_2](BF_4)_2$

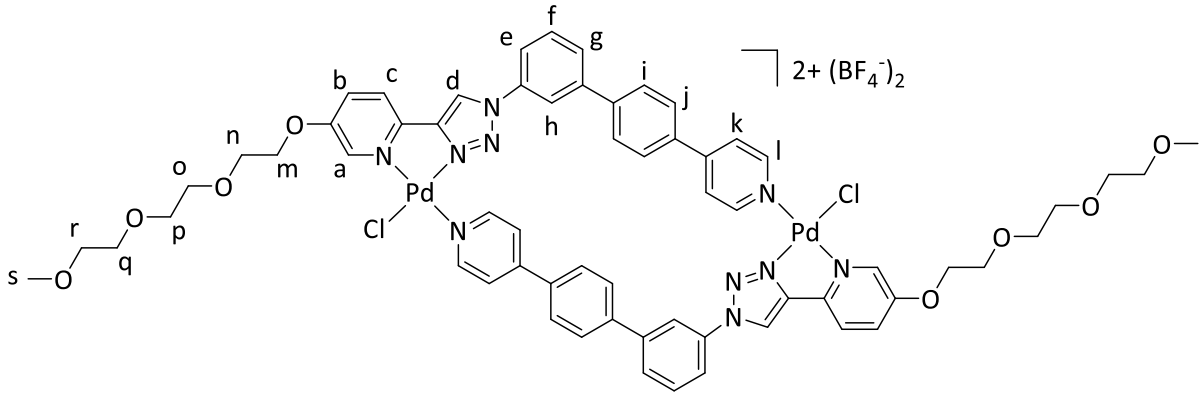

A combination of $[Pd(CH_3CN)_2Cl_2]$ (2.4 mg, 6.7 µmol) and $AgBF_4$ (1.8 mg, 6.7 µmol) in $[D_3]$acetonitrile was stirred in the absence of light for 30 minutes. To this was added **L** (3.6 mg, 6.7 µmol), and the mixture stirred in the absence of light at 40 °C for one hour. After centrifugation (4000 RPM, 10 minutes), the pellet was discarded. Vapour diffusion of diethyl ether into the filtrate provided the product as white solid (8.5 mg, 5.6 µmol, 83%). ^{1}H NMR (600 MHz, CD_3CN, 298 K) *integration given per ligand δ*: 9.05 (1H, s, H_d), 8.73 (3H, m, $H_{a,l}$), 7.96 – 7.94 (2H, m, $H_{c,h}$), 7.84 (1H, d, *J* = 8.6, H_b), 7.70 (2H, d, *J* = 5.7 Hz, H_k), 7.66 – 7.57 (7H, m, $H_{e,f,g,i,j}$), 4.26 (2H, br, H_m), 3.86 (2H, br, H_n), 3.69 – 3.68 (2H, m, H_o), 3.63 – 3.59 (4H, m, $H_{p,q}$), 3.50 – 3.48 (2H, m, H_r), 3.31 (3H, s, H_s). The low concentration precluded the collection of a ^{13}C NMR spectrum. HR ESI-MS (DMSO/DMF) *m/z* = 679.1129 $[M - 2BF_4]^{2+}$ (calc. for $C_{64}H_{64}Cl_2N_{10}O_8Pd_2$, 678.1102), *m/z* = 1445.2333 $[M - BF_4^-]^+$ (calc. for $C_{64}H_{64}BF_4Cl_2N_{10}O_8Pd_2$, 1445.2246). IR ($cm^{-1}$) 3076, 2874, 1616, 1588, 1568, 1479, 1466, 1288, 1262, 1241, 1048, 1024, 1007, 819, 787, 755.

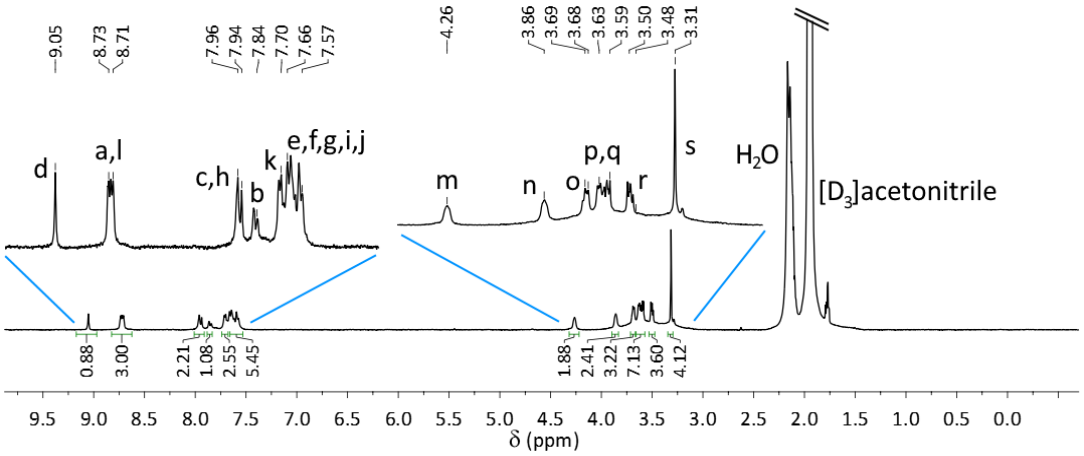

Figure 2.20 ^{1}H NMR spectrum (600 MHz, $[D_3]$acetonitrile, 298 K) of $[Pd_2L_2Cl_2](BF_4)_2$.

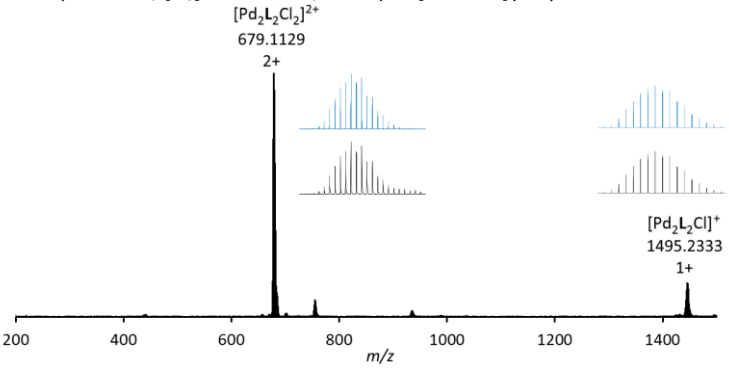

Figure 2.21 Partial mass spectrum (DMSO/DMF) of $[Pd_2L_2Cl_2](BF_4)_2$.

2.9 *In situ* generation of $[Pd_2L_2(halide)_2](BF_4)_2$ and reversal back to $[Pd_2L_2(solvent)_2](BF_4)_4$

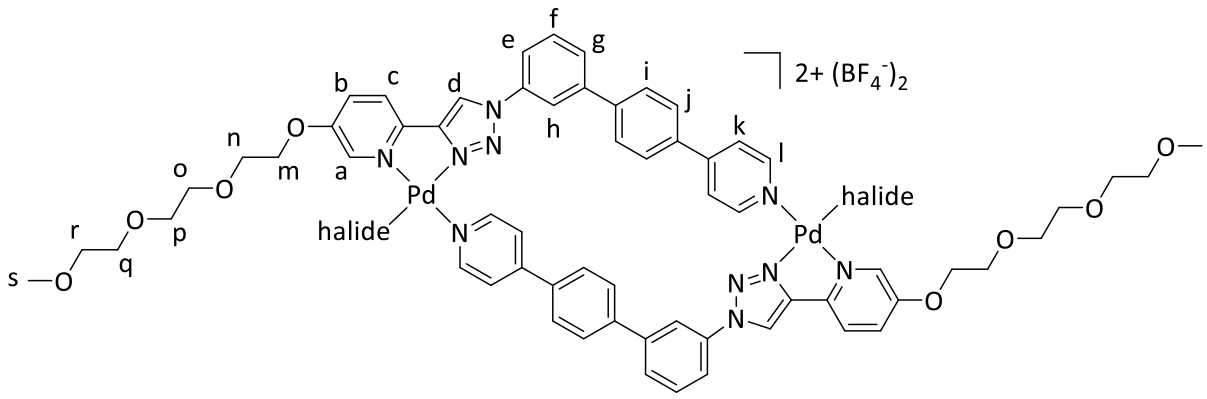

The general procedure for the formation of $[Pd_2\mathbf{L}_2(halide)_2](BF_4)_2$ complexes was as follows: a 2.5 mM solution of $[Pd_2\mathbf{L}_2(solvent)_2](BF_4)_4$ in [D$_3$]acetonitrile or [D$_6$]DMSO was treated with 2 equivalents of a halide source (Cl^-: tetraethylammonium chloride, Br^-: tetraethylammonium bromide, I^-: KI). Reversal (or attempted reversal for chloride) was carried out in [D$_6$]DMSO, through introduction of 2 equivalents of $AgBF_4$, followed by centrifugation (4000 RPM, 10 minutes) and removal of the pellet.

2.9.1 $[Pd_2L_2Cl_2](BF_4)_2$

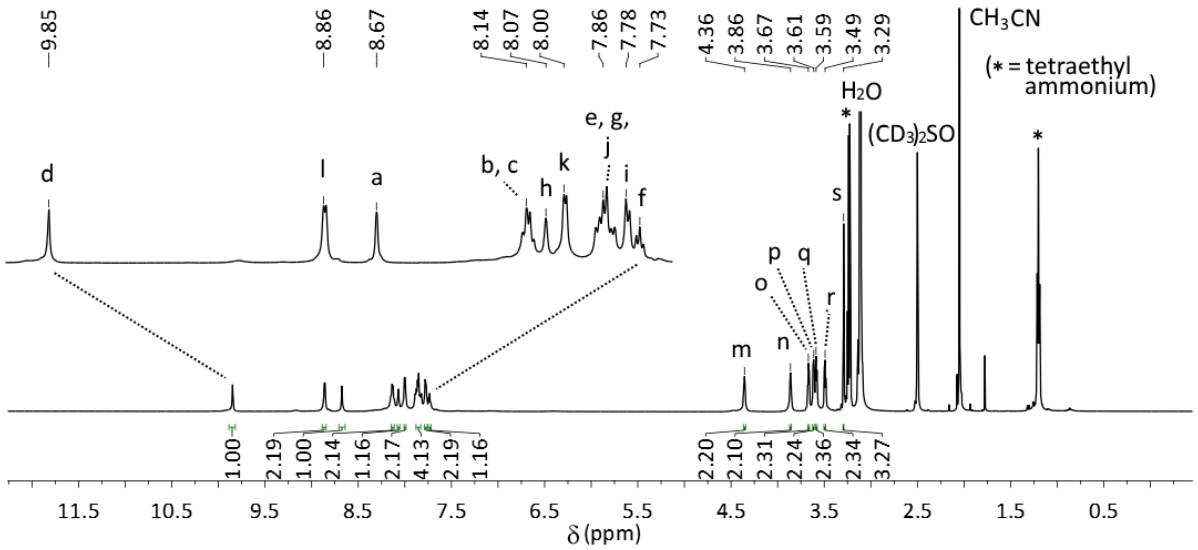

Figure 2.22 ^{1}H NMR spectrum (600 MHz, [D$_6$]DMSO, 348 K) of $[Pd_2\mathbf{L}_2Cl_2](BF_4)_2$, generated *in situ* from addition of tetramethylammonium chloride.

2.9.2 $[Pd_2L_2Br_2](BF_4)_2$

In situ solution phase characterisation: ^{1}H NMR (600 MHz, [D$_6$]DMSO, 298 K) *integration given per ligand δ*: 9.92 (1H, s, H_d), 8.86 – 8.84 (3H, m, $H_{a,l}$), 8.20 (1H, d, J = 9.0 Hz, H_b), 8.09 (1H, d, J = 8.6 Hz, H_c), 8.01 – 7.99 (3H, m, $H_{h,k}$), 7.86 – 7.80 (6H, m, $H_{e,g,i,j}$), 7.67 (1H, t, J = 7.8 Hz, H_f), 4.32 (2H, br, H_m), 3.83 (2H, br, H_n), 3.66 – 3.63 (2H, m, H_o), 3.59 – 3.54 (4H, m, $H_{p,q}$), 3.47 – 3.45 (2H, m, H_r), 3.26 (3H, s, H_s). HR ESI-MS (DMSO/DMF) *m/z* = 724.0850 $[M - 2BF_4]^{2+}$ (calc. for $C_{64}H_{64}BBr_2F_4N_{10}O_8Pd_2$, 724.0593).

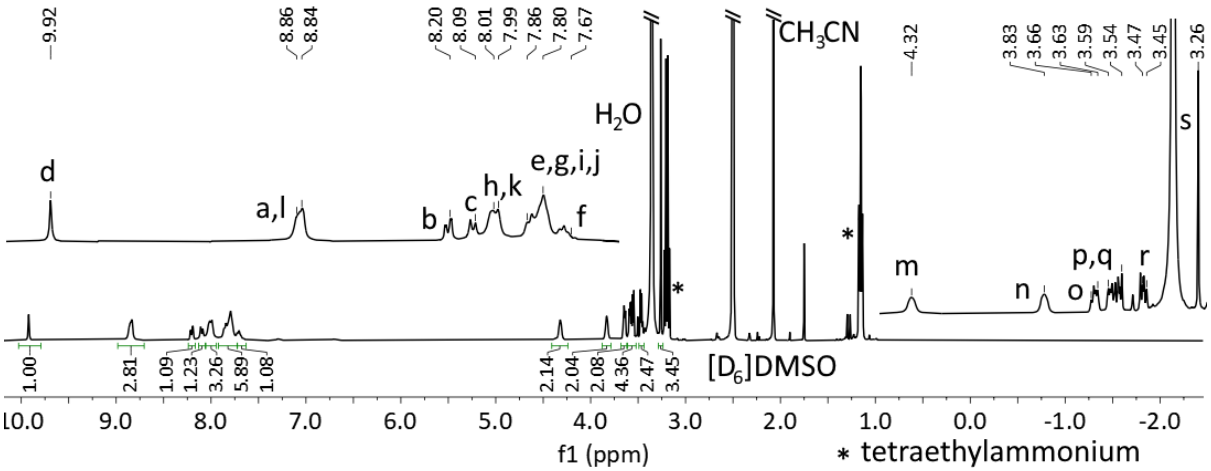

Figure 2.23 ^{1}H NMR spectrum (600 MHz, [D$_6$]DMSO, 298 K) of [Pd$_2$**L**$_2$Br$_2$](BF$_4$)$_2$, generated *in situ* from addition of tetramethylammonium bromide.

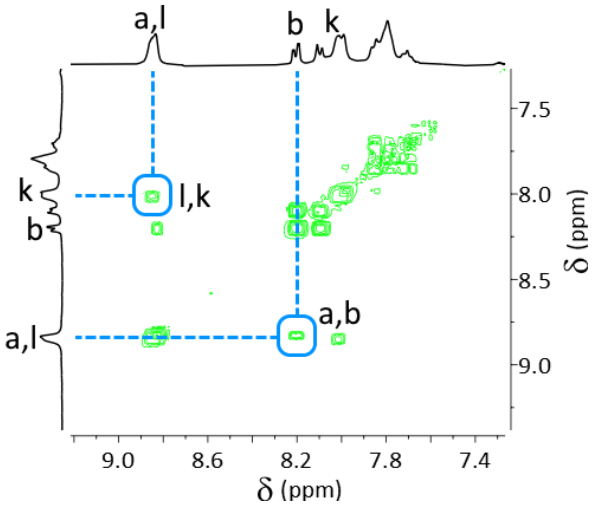

Figure 2.24 Partial ^{1}H 2D TOCSY NMR (600 MHz, [D$_6$]DMSO, 298 K) of [Pd$_2$**L**$_2$Br$_2$](BF$_4$)$_2$, generated *in situ* from [Pd$_2$**L**$_2$DMSO$_2$]$^{4+}$ and tetraethylammonium bromide.

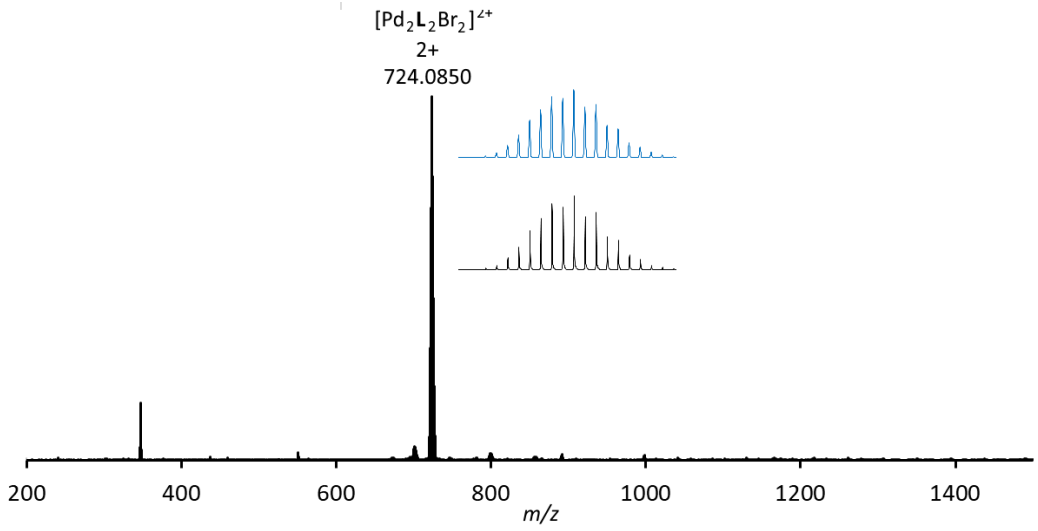

Figure 2.25 Partial mass spectrum (DMSO/DMF) of [Pd$_2$**L**$_2$Br$_2$](BF$_4$)$_2$.

2.9.3 $[Pd_2L_2I_2](BF_4)_2$

In situ solution phase characterisation: ^{1}H NMR (600 MHz, [D_6]DMSO, 298 K) *integration given per ligand δ*: 9.43 (1H, s, H_a), 9.12 (1H, s, H_d), 8.88 (2H, br, H_l), 8.02 (2H, br, $H_{c,h}$), 7.89 (1H, d, *J* = 8.2 Hz, H_b), 7.79 – 7.64 (9H, m, $H_{e,f,g,k,i,j}$), 4.32 (2H, br, H_m), 3.89 (2H, br, H_n), 3.71 – 3.69 (2H, m, H_o), 3.65 – 3.60 (4H, m, $H_{p,q}$), 3.52 – 3.50 (2H, m, H_r), 3.33 (3H, s, H_s). HR ESI-MS (DMSO/DMF) *m/z* = 771.0446 [M – $2BF_4$]$^{2+}$ (calc. for $C_{64}H_{64}BF_4I_2N_{10}O_8Pd_2$, 771.0465).

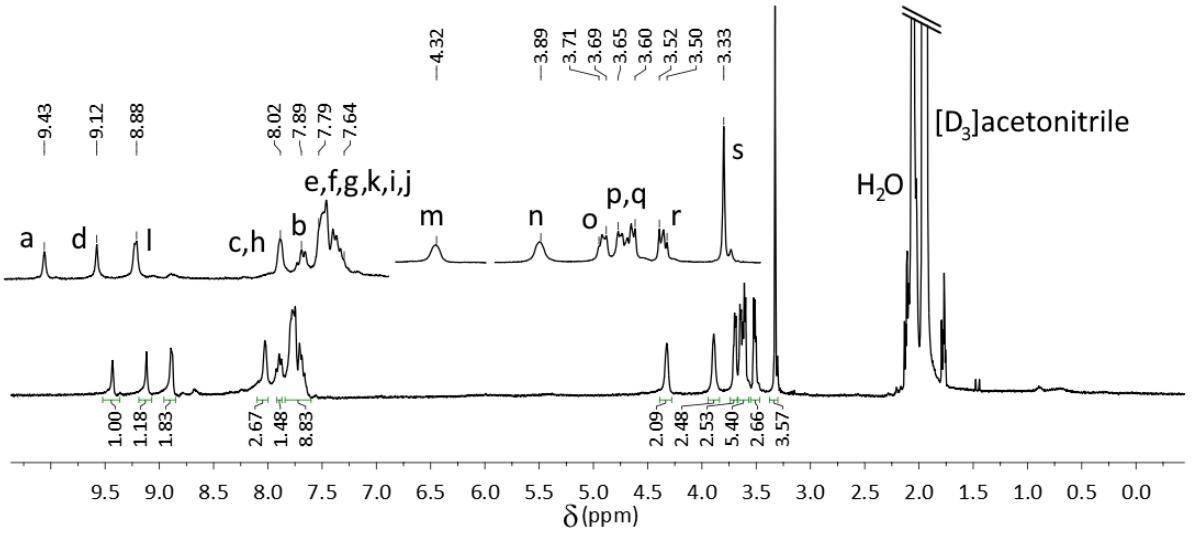

Figure 2.26 ^{1}H NMR spectrum (600 MHz, [D_3]acetonitrile, 298 K) of $[Pd_2\mathbf{L}_2I_2](BF_4)_2$, generated *in situ* from addition of potassium iodide.

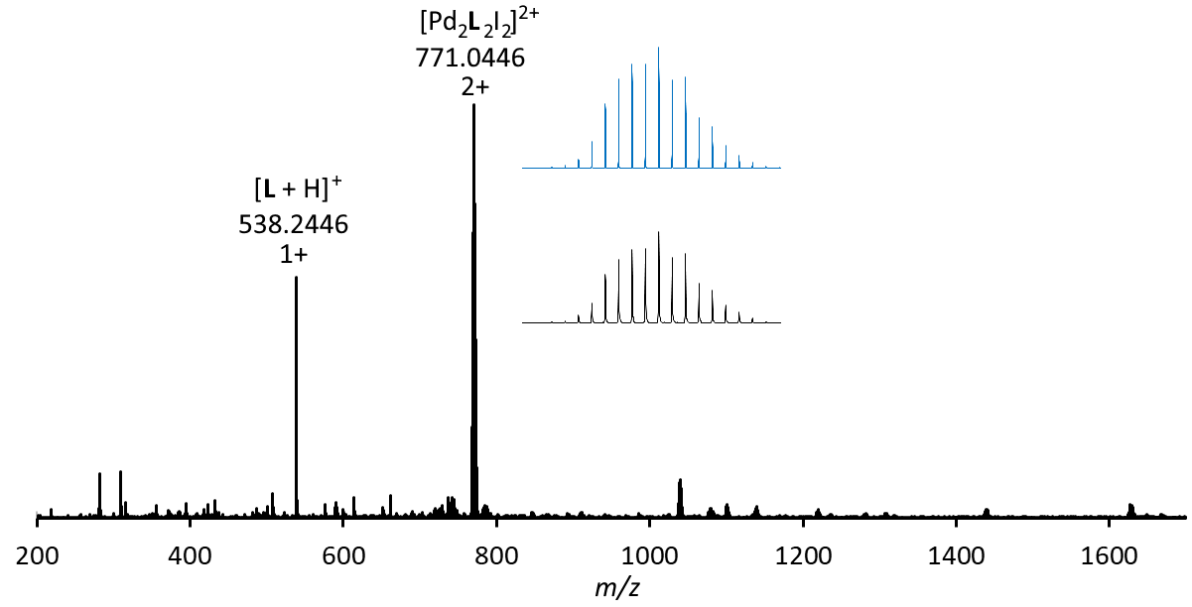

Figure 2.27 Partial mass spectrum (DMSO/DMF) of $[Pd_2\mathbf{L}_2Cl_2](BF_4)_2$.

2.9.4 Switching

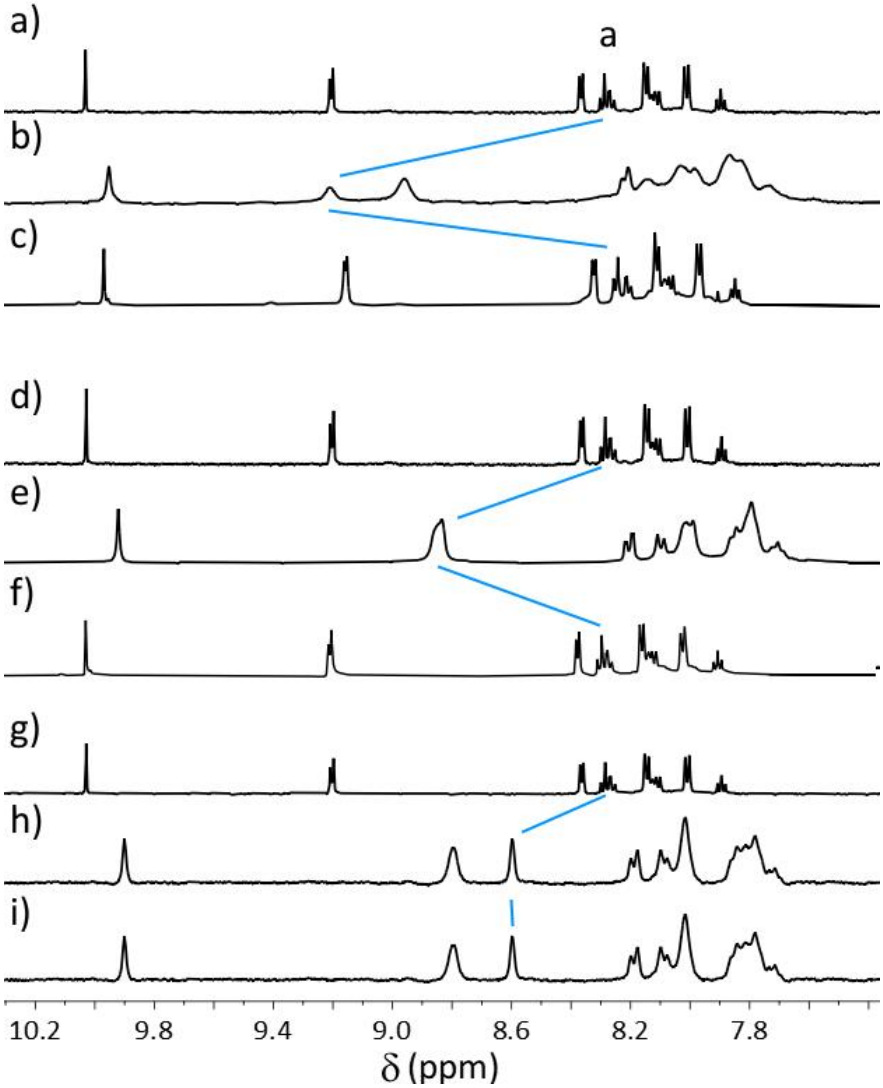

Figure 2.28 Partial stacked ^{1}H NMR spectra (600 MHz, [D_6]DMSO, 298 K) for a) $[Pd_2\mathbf{L}_2DMSO_2]^{4+}$, b) $[Pd_2\mathbf{L}_2DMSO_2]^{4+}$ + 2 eq. I^-, c) $[Pd_2\mathbf{L}_2DMSO_2]^{4+}$ + 2 eq. I^- + 2 eq. $AgBF_4$, d) $[Pd_2\mathbf{L}_2DMSO_2]^{4+}$, e) $[Pd_2\mathbf{L}_2DMSO_2]^{4+}$ + 2 eq. Br^-, f) $[Pd_2\mathbf{L}_2DMSO_2]^{4+}$ + 2 eq. Br^- + 2 eq. $AgBF_4$, g) $[Pd_2\mathbf{L}_2DMSO_2]^{4+}$, h) $[Pd_2\mathbf{L}_2DMSO_2]^{4+}$ + 2 eq. Cl^-, i) $[Pd_2\mathbf{L}_2DMSO_2]^{4+}$ + 2 eq. Cl^- + 2 eq. $AgBF_4$. The spectrum in i) did not change after being left to stand for days, or after heating (60 °C) overnight.

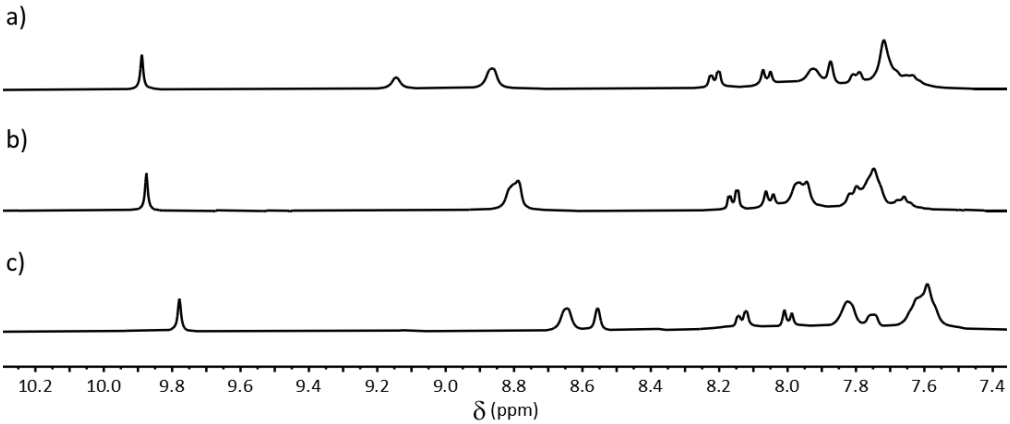

Figure 2.29 Partial stacked ^{1}H NMR spectra (400 MHz, [D_6]DMSO, 298 K) at [complex] = 20 mM for a) $[Pd_2\mathbf{L}_2I_2]^{2+}$, b) $[Pd_2\mathbf{L}_2Br_2]^{2+}$, and c) $[Pd_2\mathbf{L}_2Cl_2]^{2+}$.

2.10 VT NMR spectra for $[Pd_2L_2(halide)_2](BF_4)_2$ complexes

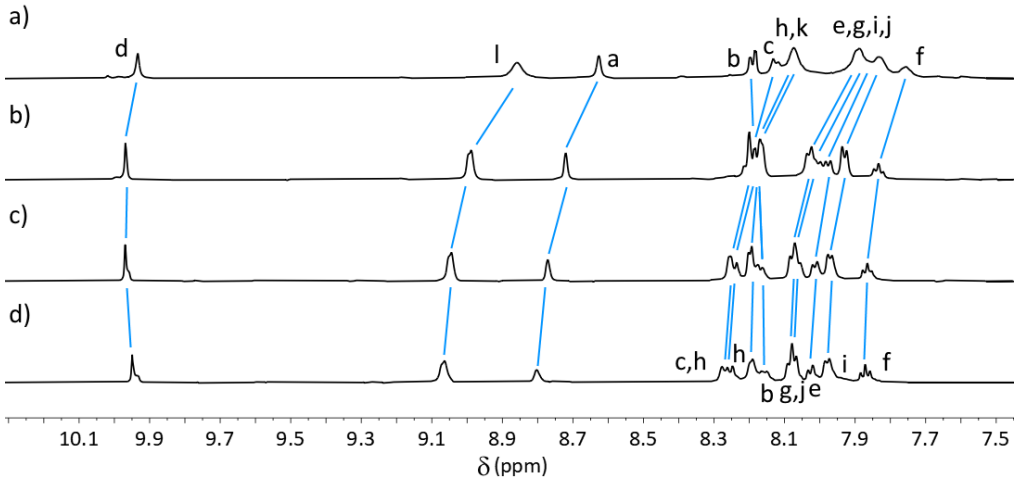

Figure 2.30 Partial stacked ^{1}H NMR spectra (600 MHz, [D$_6$]DMSO) for $[Pd_2\mathbf{L}_2Cl_2](BF_4)_2$ at a) 298 K, and b) 323 K, c) 348 K, and d) 373 K.

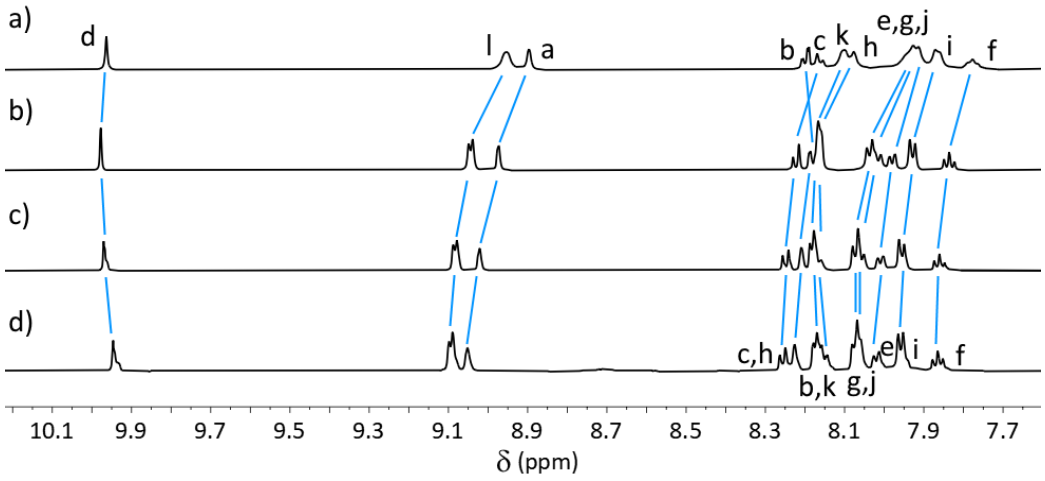

Figure 2.31 Partial stacked ^{1}H NMR spectra (600 MHz, [D$_6$]DMSO) for $[Pd_2\mathbf{L}_2Br_2](BF_4)_2$ at a) 298 K, b) 323 K, c) 348 K and d) 373 K.

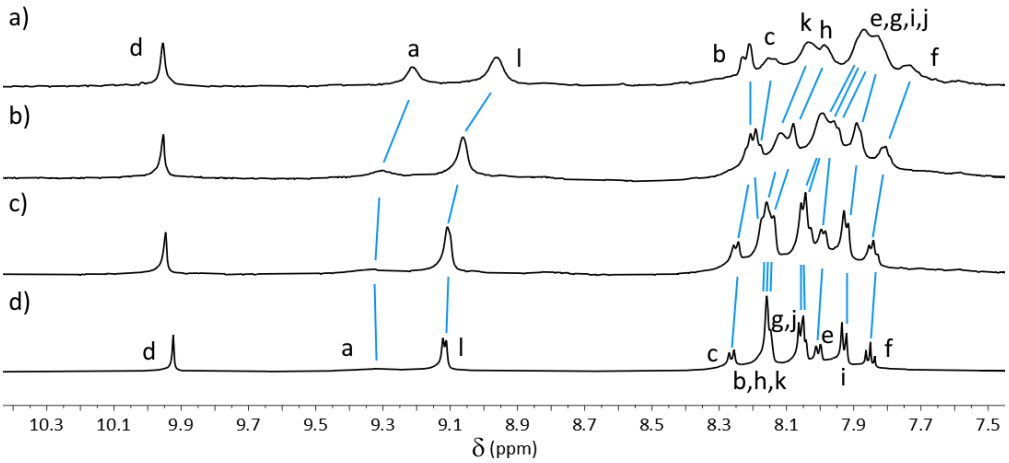

Figure 2.32 Partial stacked ^{1}H NMR spectra (600 MHz, [D$_6$]DMSO) for $[Pd_2\mathbf{L}_2I_2](BF_4)_2$ at a) 298 K, b) 323 K, c) 348 K, and d) 373 K.

2.11 1:1 $[Pd_2L_2(solvent)_2]^{4+}/[Pd_2L_2(halide)_2]^{2+}$ mixtures

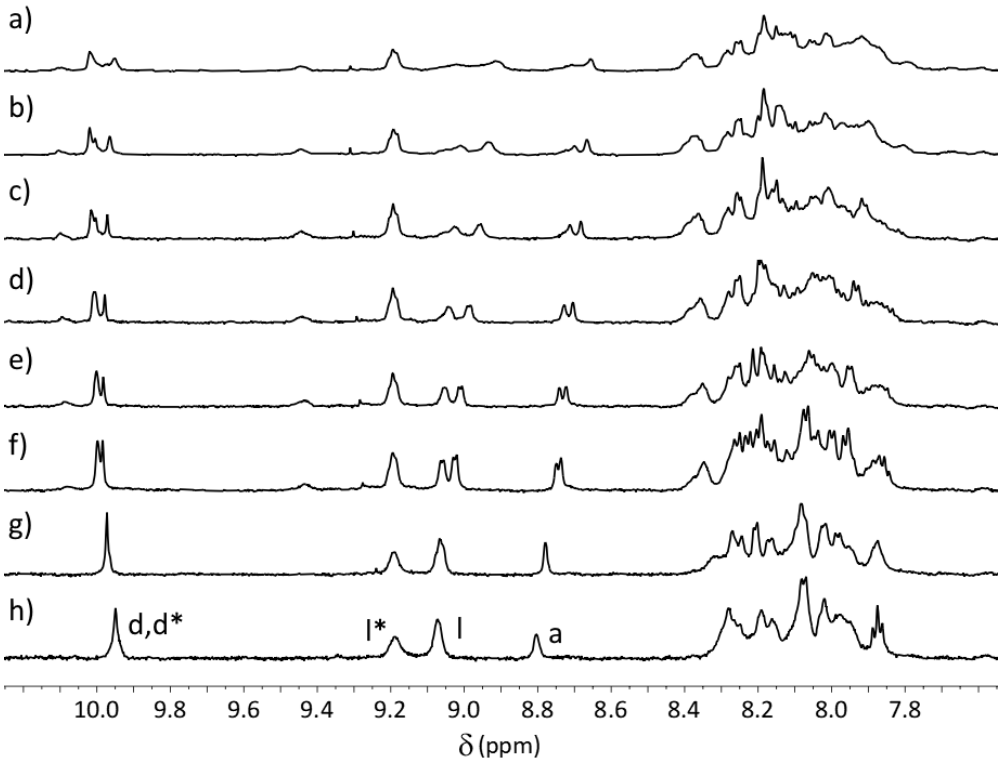

Figure 2.33 Partial ^{1}H NMR spectra (600 MHz, [D_6]DMSO) from a 1:1 combination of $[Pd_2\mathbf{L}_2(solvent)_2]^{4+}$ and $[Pd_2\mathbf{L}_2Cl_2]^{2+}$ at a) 298 K after 10 minutes, b) 298 K after 20 minutes (equilibrated), c) 303 K, d) 310 K, e) 317 K, f) 323 K, g) 348 K, and h) 373 K. Labels with an asterisk pertain to peaks near solvent-ligated metal ions, those without to those near chloride-ligated metal ions.

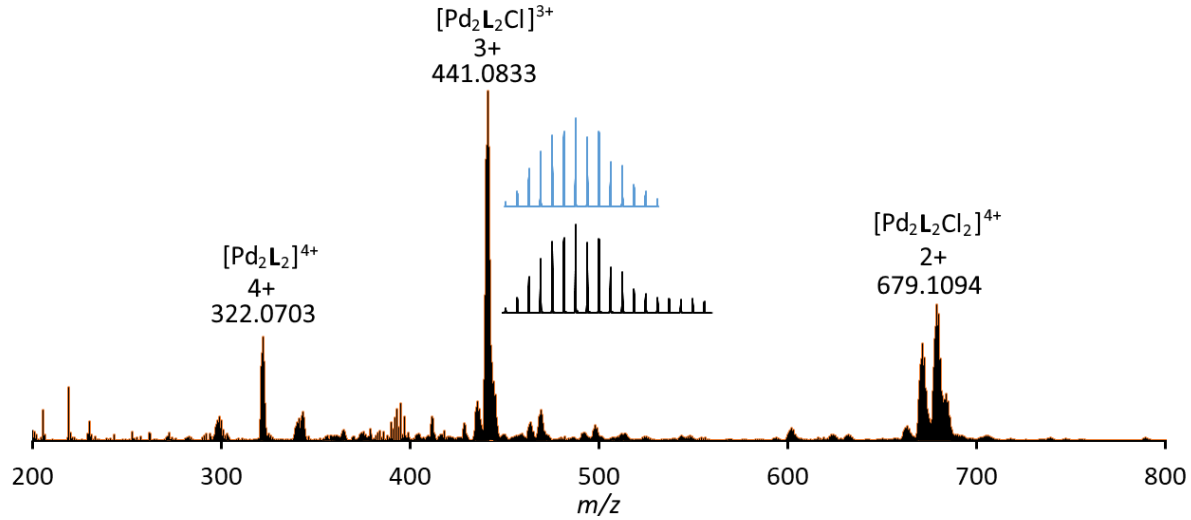

Figure 2.34 Partial mass spectrum (DMSO/acetonitrile) of the 1:1 combination of $[Pd_2\mathbf{L}_2(solvent)_2](BF_4)_4$ and $[Pd_2\mathbf{L}_2Cl_2](BF_4)_2$.

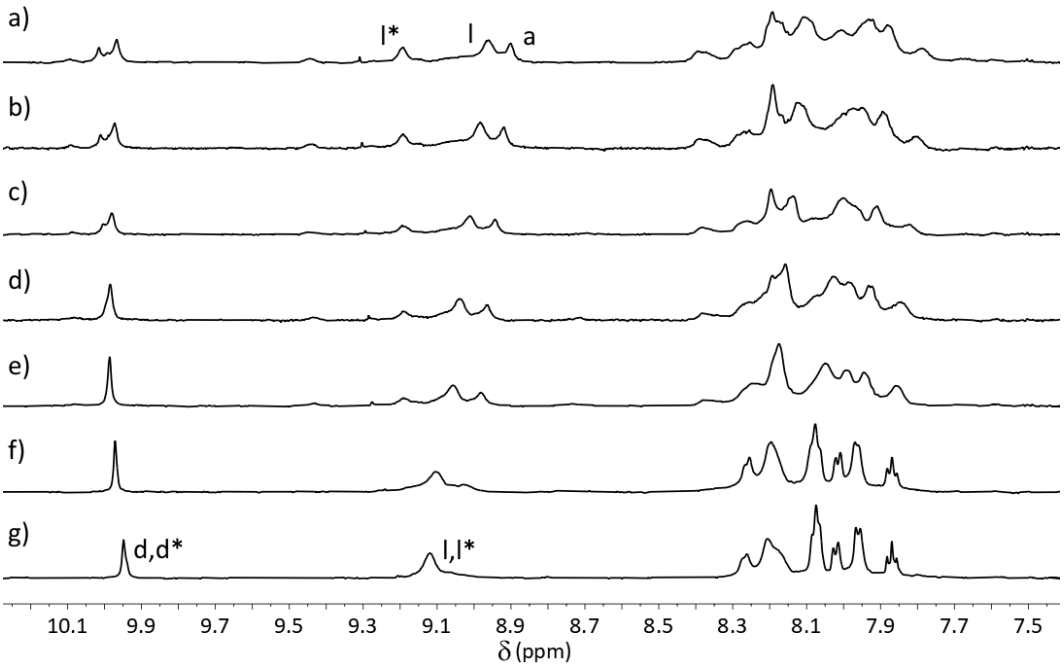

Figure 2.35 Partial ^{1}H NMR spectra (600 MHz, [D$_6$]DMSO) from a 1:1 combination of $[Pd_2\mathbf{L}_2(solvent)_2]^{4+}$ and $[Pd_2\mathbf{L}_2Br_2]^{2+}$ at a) 298 K, b) 303 K, c) 310 K, d) 317 K, e) 323 K, f) 348 K, and g) 373 K. Labels with an asterisk pertain to peaks near solvent-ligated metal ions, those without to those near bromide-ligated metal ions.

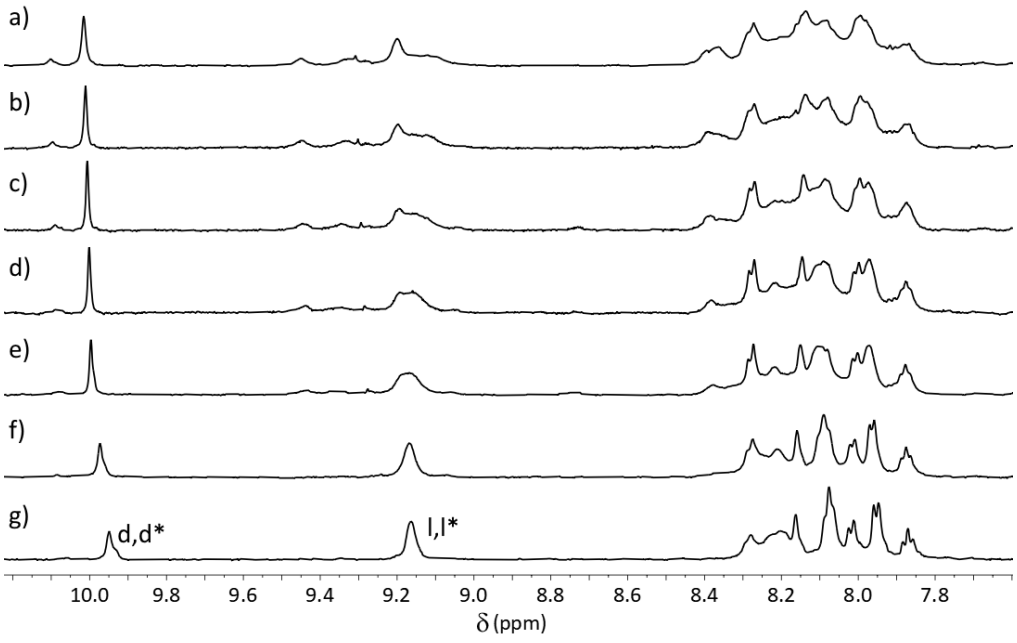

Figure 2.36 Partial ^{1}H NMR spectra (600 MHz, [D$_6$]DMSO) from a 1:1 combination of $[Pd_2\mathbf{L}_2(solvent)_2]^{4+}$ and $[Pd_2\mathbf{L}_2I_2]^{2+}$ at a) 298 K, b) 303 K, c) 310 K, d) 317 K, e) 323 K, f) 348 K, and g) 373 K. Labels with an asterisk pertain to peaks near solvent-ligated metal ions, those without to those near iodide-ligated metal ions.

3 Calculations

All DFT calculations were performed using the ORCA program version 4.0.[5] All structures were fully optimized using the BP86[6-8] functional with a def2-SVP basis set.[9] The resolution of identity approximation[10] was also used in the BP86 calculations, with a def2-SVP/J auxiliary basis set.[11-13] SCF iterations were considered converged when the energy change was less than 1×10^{-8} a.u. The geometry

was considered optimized when the following tolerances were met: Gradient = 5×10^{-6} a.u., RMS gradient = 1×10^{-4} a.u., maximum gradient = 3×10^{-4} a.u., RMS displacement = 2×10^{-3} a.u., maximum displacement = 4×10^{-3} a.u.. To reduce numerical error in the DFT integration, more grid points were used for both the angular and radial grids via the keyword "Grid4" for the SCF iterations and for the final energy evaluation. A CPCM indefinite field solvent field was applied. For $[\mathbf{2Pt}\subset Pd_2\mathbf{L}_2(DMSO)_2]^{4+}$, the **2Pt** guest was allowed to optimise, and the host coordinates were fixed from the DFT-optimised structure. The energies for the formation of the halide complexes (obtained from products minus reactants) was -270 kJ mol^{-1} (Cl^-), -236 kJ mol^{-1} (Br^-) and -22 kJ mol^{-1} (I^-). Files available in xyz format.

4 Comparison of previously crystallographically-described complexes with DFT-structures

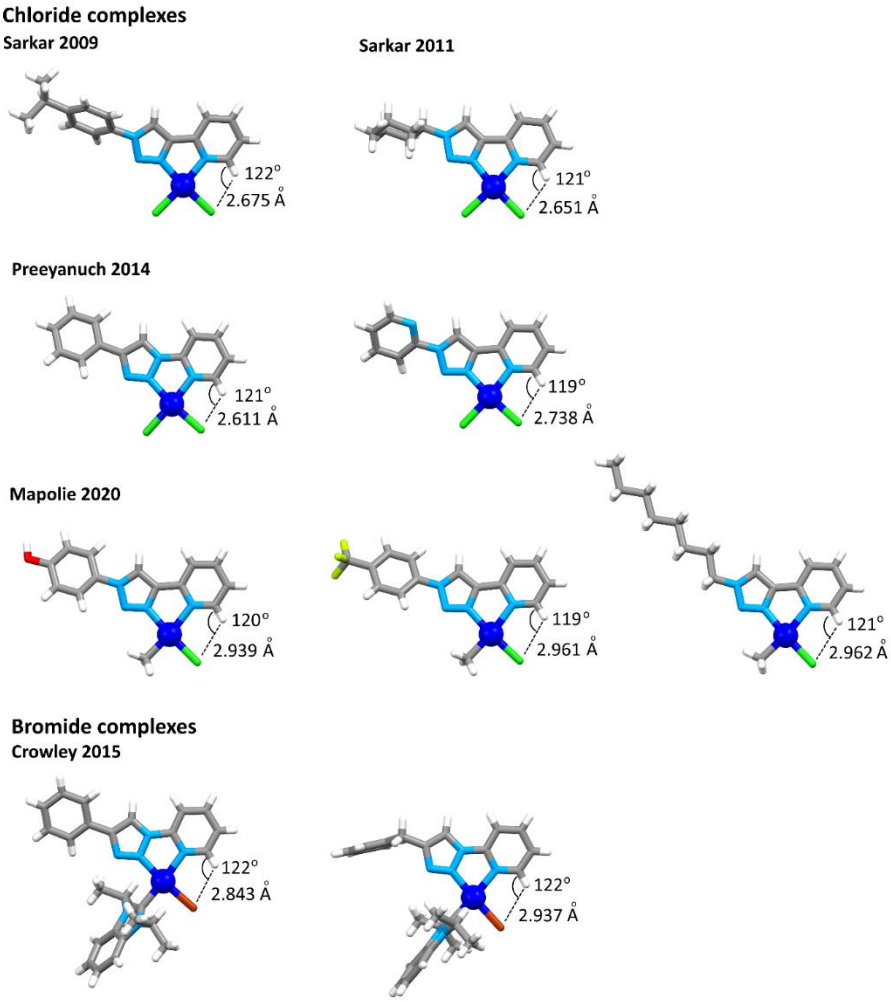

Figure 4.1 Depictions of crystal structures of previously reported complexes from 2-pyridyl-1,2,3-triazole with a halide *cis* to the pyridine from the bidentate chelator. D-H---A angle and A---H distance shown for each example.[14-18] Colours: carbon grey, hydrogen white, bromine brown, chlorine green, fluorine lime, oxygen red, palladium dark blue.

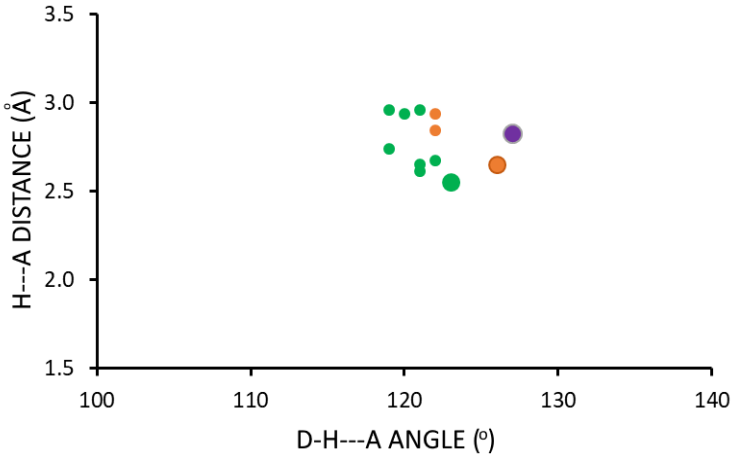

Figure 4.2 Plot of the H---A distances and D-H---A angles from crystal structures from the literature (see **Figure 4.1**) and DFT –optimised structures for $[Pd_2\mathbf{L}_2(halide)_2]^{2+}$ complexes in this study. Colours: green chloride, brown bromide, purple iodide, small circles from crystal structures, large circles from DFT-optimised structures.

5 Host-guest chemistry

5.1 General titration information

Solutions of the host at 2.5 mM in $[D_6]$DMSO or $[D_3]$acetonitrile were treated with aliquots of equal volume of host (5.0 mM) and the guest, both in the same solvent, such that the overall concentration of host remained constant and the concentration of the guest increased with each aliquot. Calculated equivalencies were compared to those observed via integration in the ^{1}H NMR spectra, with good agreement.

5.2 Host-guest chemistry with 2Pt

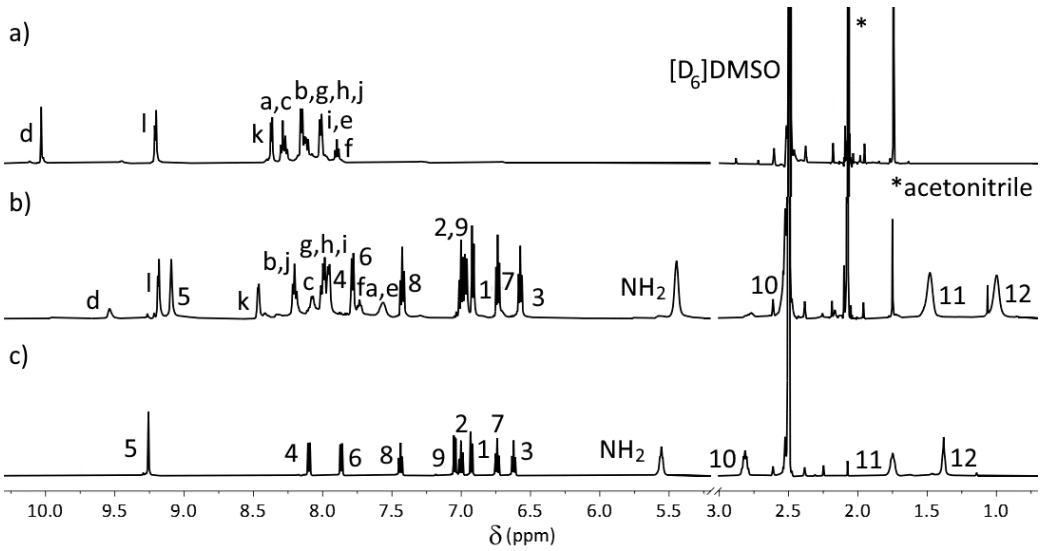

Figure 5.1 Partial stacked ^{1}H NMR spectra (600 MHz, $[D_6]$DMSO, 298 K) of a) $[Pd_2\mathbf{L}_2(DMSO)_2]^{4+}$ at 2.5 mM, b) $[Pd_2\mathbf{L}_2(DMSO)_2]^{4+}$ at 2.5 mM + 2 eq. **2Pt**, and c) **2Pt**.

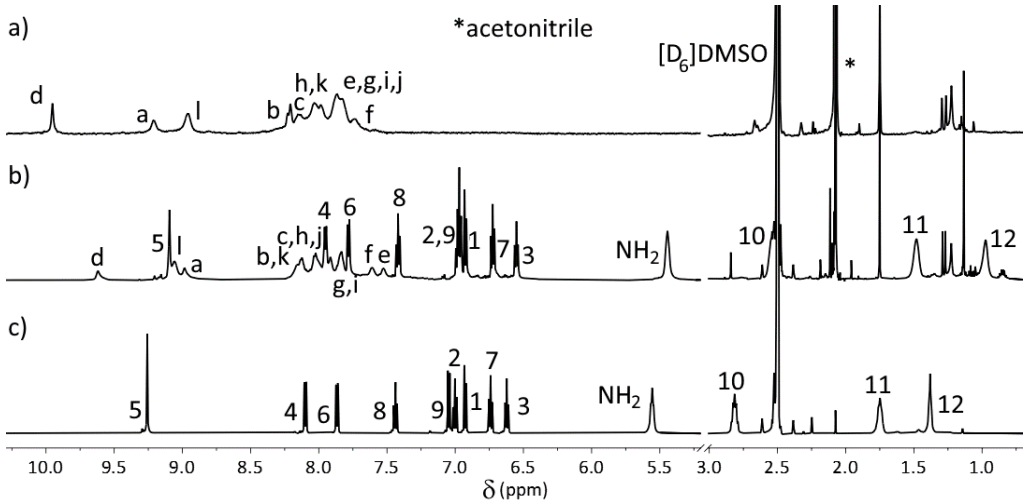

Figure 5.2 Partial stacked ^{1}H NMR spectra (600 MHz, [D$_6$]DMSO, 298 K) of a) $[Pd_2\mathbf{L}_2I_2]^{2+}$ at 2.5 mM, b) $[Pd_2\mathbf{L}_2I_2]^{2+}$ at 2.5 mM + 2 eq. **2Pt**, and c) **2Pt**.

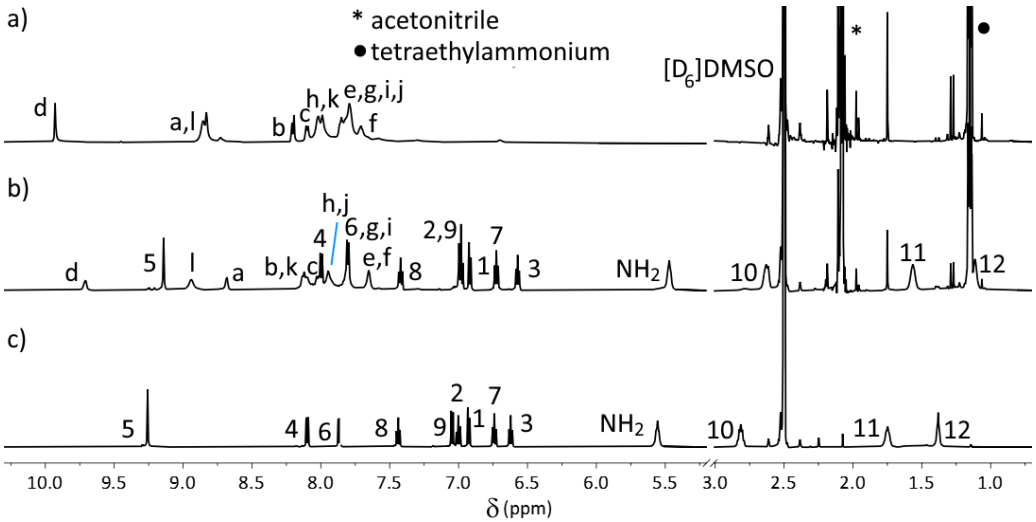

Figure 5.3 Partial stacked ^{1}H NMR spectra (600 MHz, [D$_6$]DMSO, 298 K) of a) $[Pd_2\mathbf{L}_2Br_2]^{2+}$ at 2.5 mM, b) $[Pd_2\mathbf{L}_2Br_2]^{2+}$ at 2.5 mM + 2 eq. **2Pt**, and c) **2Pt**.

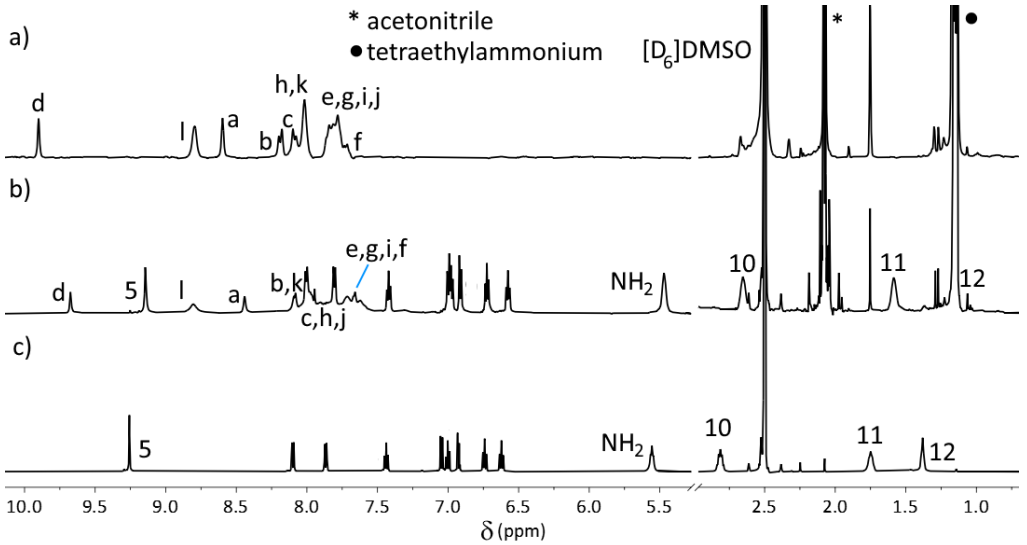

Figure 5.4 Partial stacked ^{1}H NMR spectra (600 MHz, [D$_6$]DMSO, 298 K) of a) $[Pd_2\mathbf{L}_2Cl_2]^{2+}$ at 2.5 mM, b) $[Pd_2\mathbf{L}_2Cl_2]^{2+}$ at 2.5 mM + 2 eq. **2Pt**, and c) **2Pt**.

5.2.1 2D ^{1}H NMR spectroscopic data

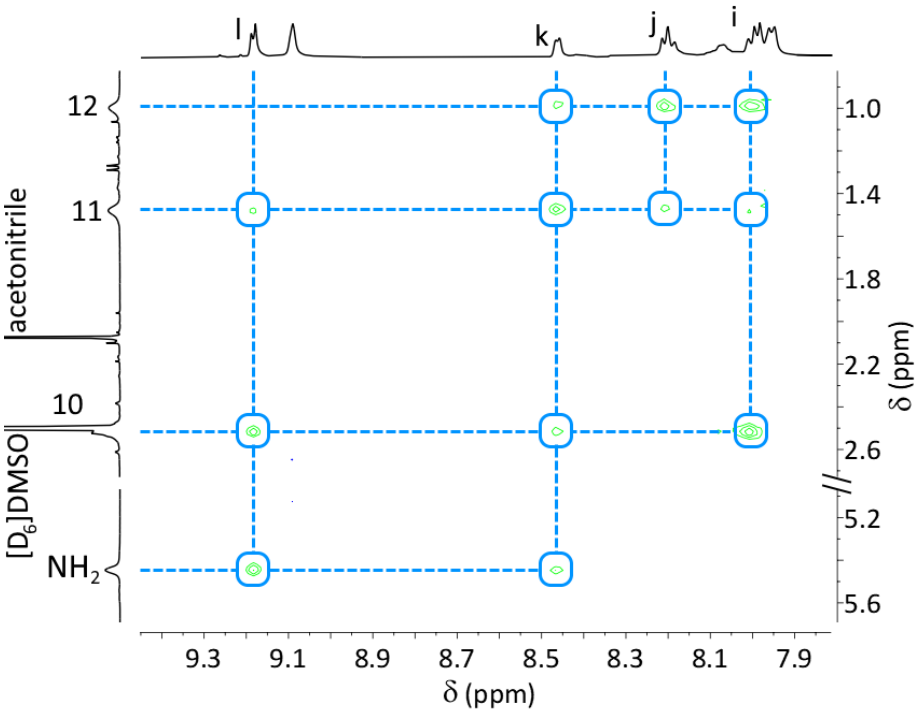

Figure 5.5 Partial ^{1}H 2D NOESY NMR spectrum (600 MHz, [D_6]DMSO, 298 K, 300 ms mixing time) of [(**2Pt**)$_2$⊂Pd$_2$**L**$_2$(DMSO)$_2$]$^{4+}$ showing through-space interactions between the alkyl chain of the guest and the phenylpyridine arms of the host.

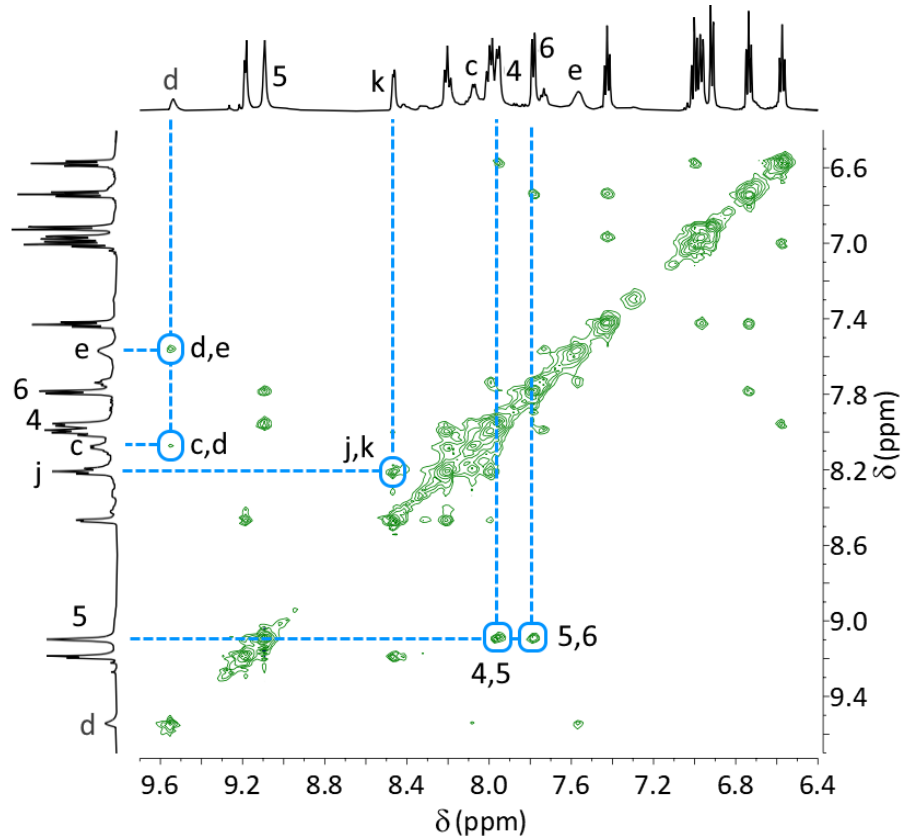

Figure 5.6 Partial ^{1}H 2D NOESY NMR spectrum (600 MHz, [D_6]DMSO, 298 K, 300 ms mixing time) of [(**2Pt**)$_2$⊂Pd$_2$**L**$_2$(DMSO)$_2$]$^{4+}$ showing through-space interactions allowing assignment of key peaks in both structures.

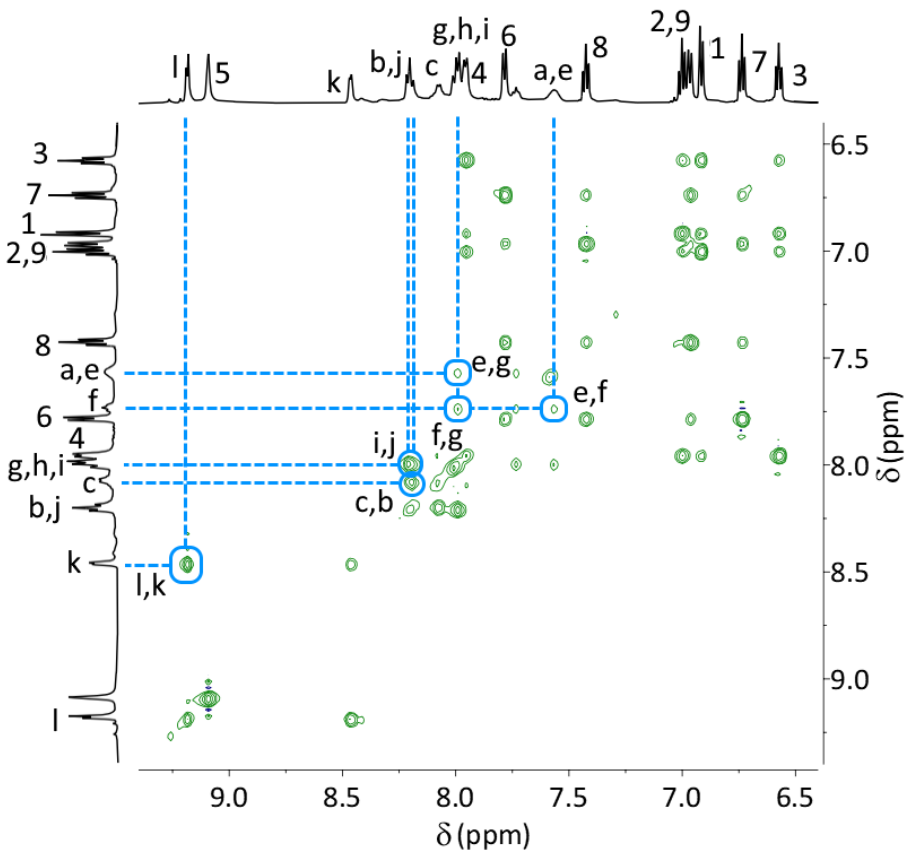

Figure 5.7 Partial ^{1}H 2D TOCSY NMR spectrum (600 MHz, [D$_6$]DMSO, 298 K) of [(**2Pt**)$_2$⊂Pd$_2$**L**$_2$(DMSO)$_2$]$^{4+}$.

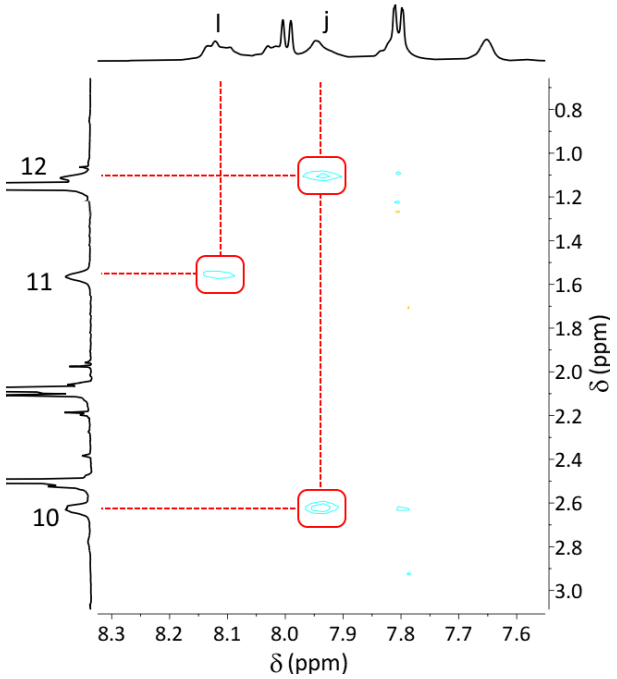

Figure 5.8 Partial ^{1}H 2D NOESY NMR spectrum (600 MHz, [D$_6$]DMSO, 298 K, 300 ms mixing time) of [(**2Pt**)$_2$⊂Pd$_2$**L**$_2$Br$_2$]$^{2+}$ showing through-space interactions between the alkyl chain of the guest and the phenyl rings on the arms of the host.

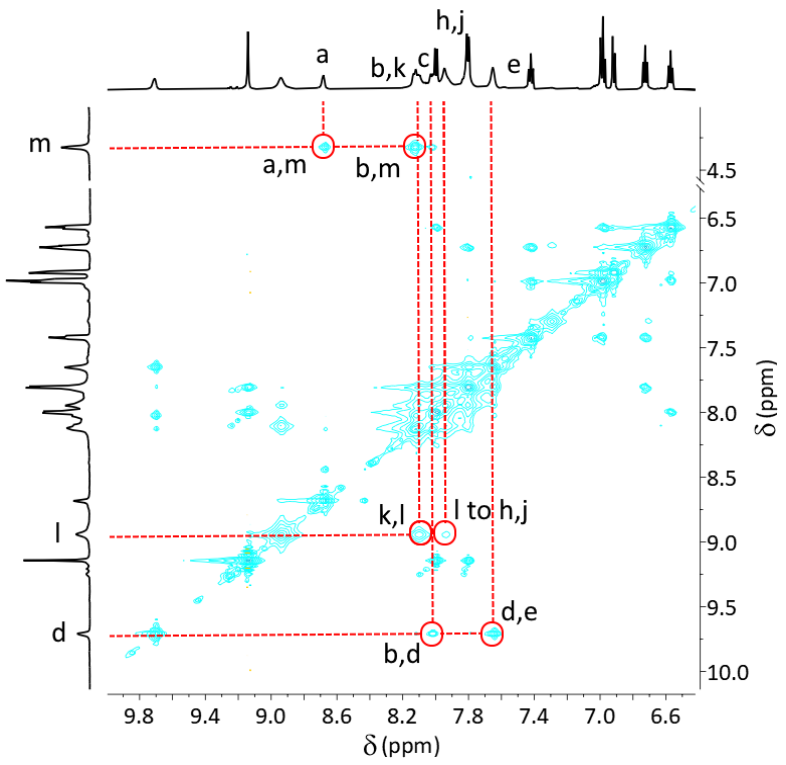

Figure 5.9 Partial ^{1}H 2D NOESY NMR spectrum (600 MHz, [D$_6$]DMSO, 298 K, 300 ms mixing time) of [(**2Pt**)$_2$⊂Pd$_2$**L**$_2$Br$_2$]$^{2+}$ showing through-space interactions allowing assignment of key peaks in both structures.

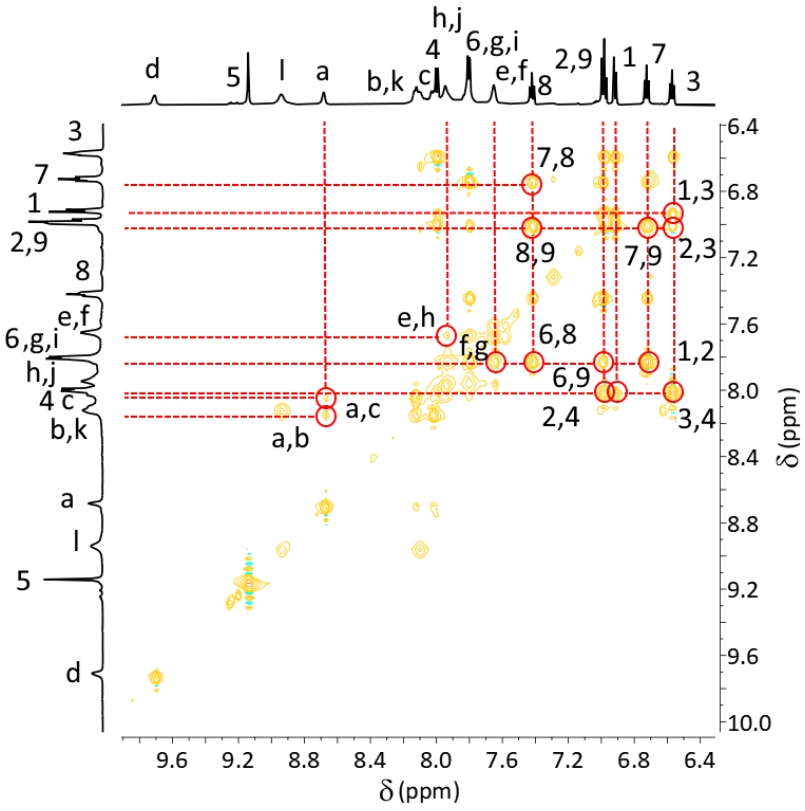

Figure 5.10 Partial ^{1}H 2D TOCSY NMR spectrum (600 MHz, [D$_6$]DMSO, 298 K) of [(**2Pt**)$_2$⊂Pd$_2$**L**$_2$Br$_2$]$^{2+}$.

5.2.2 Switching in the presence of the guest

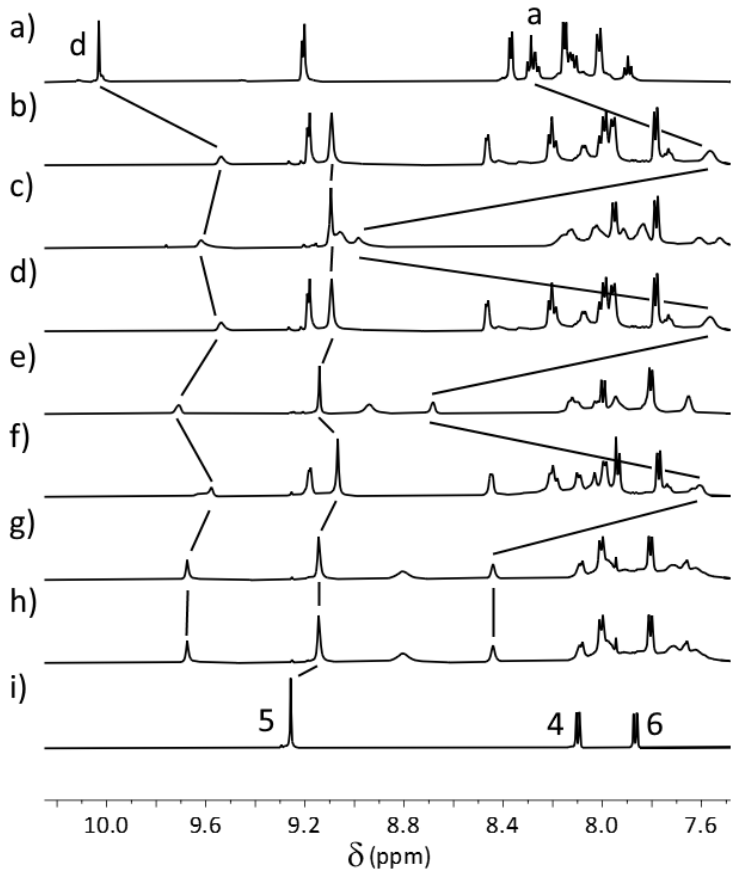

Figure 5.11 Partial stacked ^{1}H NMR spectra (400 MHz, [D_6]DMSO, 298 K) of a) $[Pd_2\mathbf{L}_2(DMSO)_2]^{4+}$, b) + **2Pt**, giving $[\mathbf{2Pt}_2\subset Pd_2\mathbf{L}_2(DMSO)_2]^{4+}$, c) + I^-, giving $[\mathbf{2Pt}_2\subset Pd_2\mathbf{L}_2I_2]^{2+}$, d) + $AgBF_4$, giving $[\mathbf{2Pt}_2\subset Pd_2\mathbf{L}_2(DMSO)_2]^{4+}$, e) + Br^-, giving $[\mathbf{2Pt}_2\subset Pd_2\mathbf{L}_2Br_2]^{2+}$, f) + $AgBF_4$, giving $[\mathbf{2Pt}_2\subset Pd_2\mathbf{L}_2(DMSO)_2]^{4+}$, g) + Cl^-, giving $[\mathbf{2Pt}_2\subset Pd_2\mathbf{L}_2Cl_2]^{2+}$,g) after addition of $AgBF_4$, still showing $[\mathbf{2Pt}_2\subset Pd_2\mathbf{L}_2Cl_2]^{2+}$, and i) **2Pt**.

5.2.3 ^{1}H NMR titration data

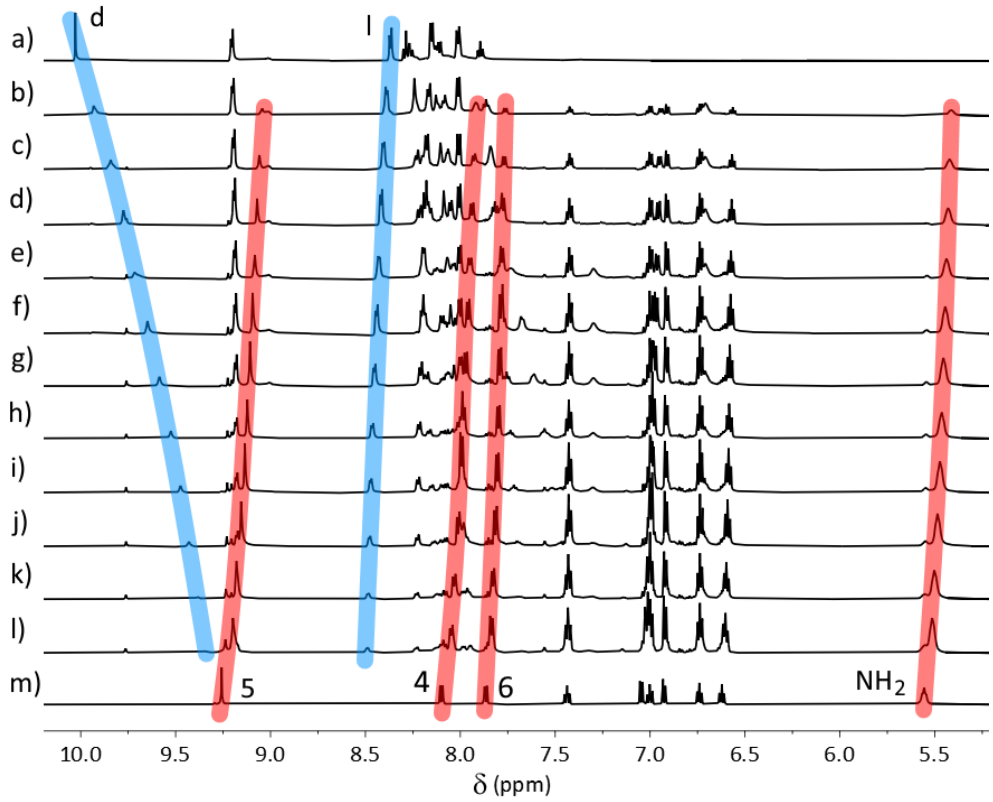

Figure 5.12 Partial stacked ^{1}H NMR spectra (600 MHz, [D_6]DMSO, 298 K) at [host] = 2.5 mM, of a) $[Pd_2\mathbf{L}_2(DMSO)_2]^{4+}$, b) + 0.3 eq. **2Pt**, c) + 0.6 eq. **2Pt**, d) + 0.9 eq. **2Pt**, e) + 1.2 eq. **2Pt**, f) + 1.5 eq. **2Pt**, g) + 1.8 eq. **2Pt**, h) + 2.6 eq. **2Pt**, i) + 3.4 eq. **2Pt**, j) + 4.0 eq. **2Pt**, k) + 5.0 eq. **2Pt**, l) + 8.0 eq. **2Pt**, and m) **2Pt**.

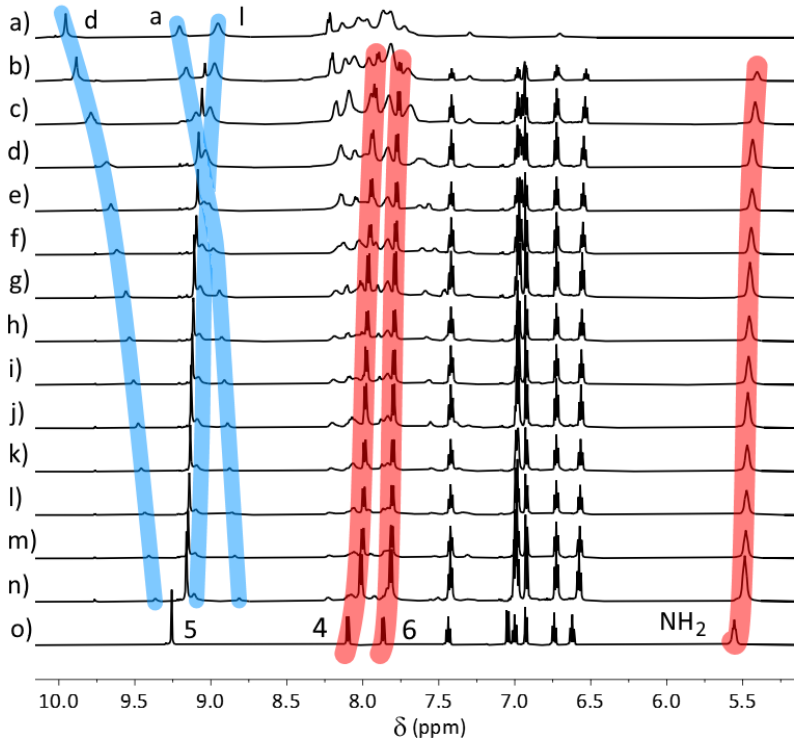

Figure 5.13 Partial stacked ^{1}H NMR spectra (600 MHz, [D_6]DMSO, 298 K) at [host] = 2.5 mM, of a) $[Pd_2\mathbf{L}_2\mathbf{I}_2]^{2+}$, b) + 0.3 eq. **2Pt**, c) + 0.6 eq. **2Pt**, d) + 1.2 eq. **2Pt**, e) + 1.5 eq. **2Pt**, f) + 1.8 eq. **2Pt**, g) + 2.4 eq. **2Pt**, h) + 2.6 eq. **2Pt**, i) + 2.8 eq. **2Pt**, j) + 3.0 eq. **2Pt**, k) + 3.9 eq. **2Pt**, l) + 4.7 eq. **2Pt**, m) + 5.5 eq. **2Pt**, n) + 7.5 eq. **2Pt**, and o) **2Pt**.

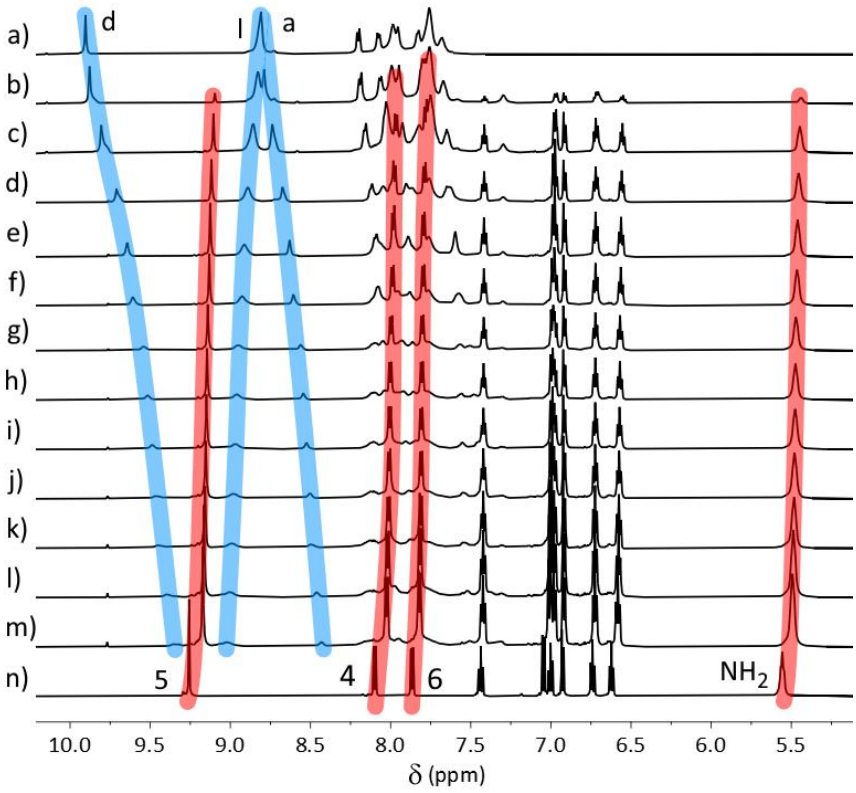

Figure 5.14 Partial stacked ^{1}H NMR spectra (600 MHz, [D$_6$]DMSO, 298 K) at [host] = 2.5 mM, of a) [Pd$_2$**L**$_2$Br$_2$]$^{2+}$, b) + 0.25 eq. **2Pt**, c) + 0.75 eq. **2Pt**, d) + 1.2 eq. **2Pt**, e) + 1.7 eq. **2Pt**, f) + 2.0 eq. **2Pt**, g) + 2.9 eq. **2Pt**, h) + 3.3 eq. **2Pt**, i) + 3.9 eq. **2Pt**, j) + 4.1 eq. **2Pt**, k) + 4.7 eq. **2Pt**, l) + 5.8 eq. **2Pt**, m) + 7.5 eq. **2Pt**, and n) **2Pt**.

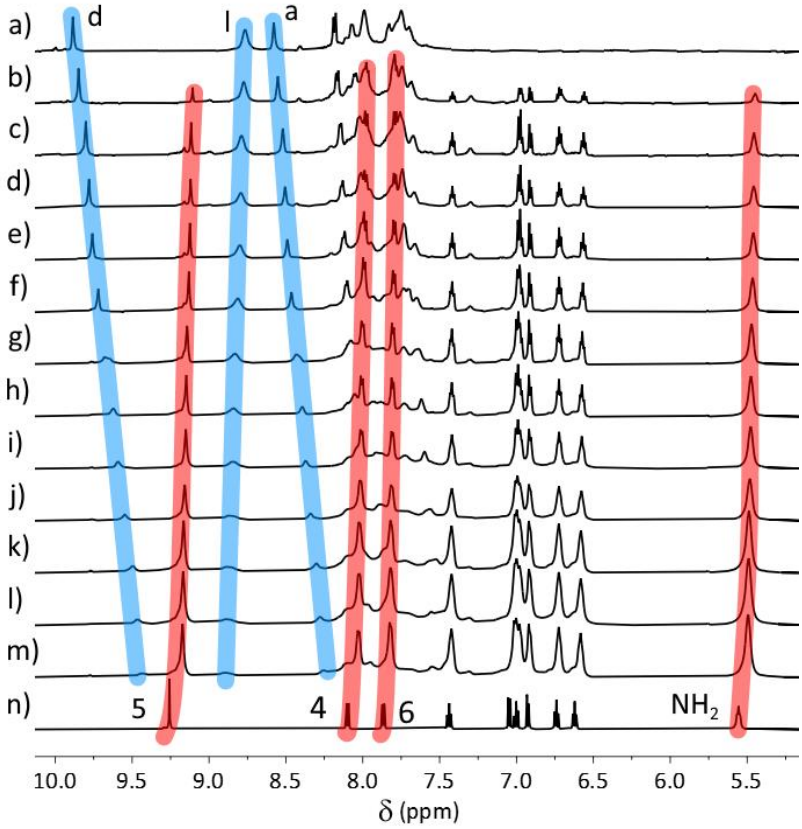

Figure 5.15 Partial stacked ^{1}H NMR spectra (600 MHz, [D$_6$]DMSO, 298 K) at [host] = 2.5 mM, of a) [Pd$_2$**L**$_2$Cl$_2$]$^{2+}$, b) + 0.25 eq. **2Pt**, c) + 0.50 eq. **2Pt**, d) + 0.75 eq. **2Pt**, e) + 1.0 eq. **2Pt**, f) + 1.3 eq. **2Pt**, g) + 2.0 eq. **2Pt**, h) + 2.8 eq. **2Pt**, i) + 3.5 eq. **2Pt**, j) + 4.0 eq. **2Pt**, k) + 5.0 eq. **2Pt**, l) + 5.7 eq. **2Pt**, m) + 7.1 eq. **2Pt**, and n) **2Pt**.

5.3 Mass spectral data

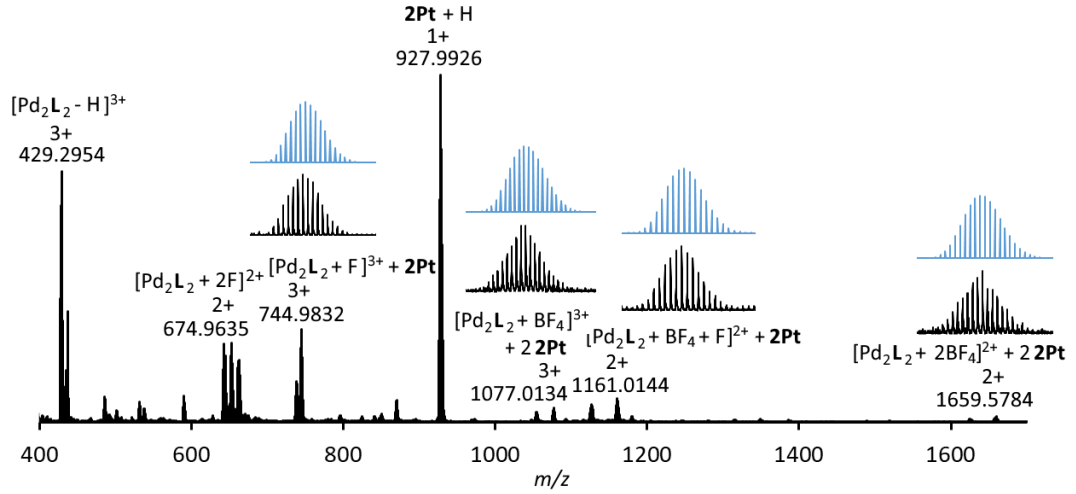

Figure 5.16 Partial mass spectrum (DMSO/acetonitrile, direct injection) of $[(\mathbf{2Pt})_2 \subset Pd_2\mathbf{L}_2(DMSO)_2]^{4+}$.

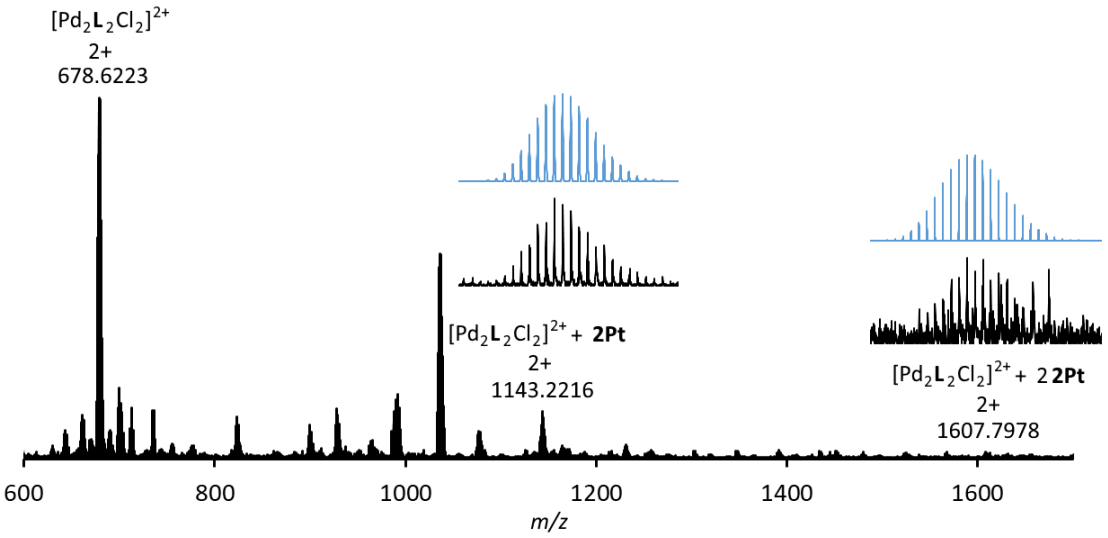

Figure 5.17 Partial mass spectrum (DMSO/acetonitrile, direct injection) of $[(\mathbf{2Pt})_2 \subset Pd_2\mathbf{L}_2Cl_2]^{2+}$.

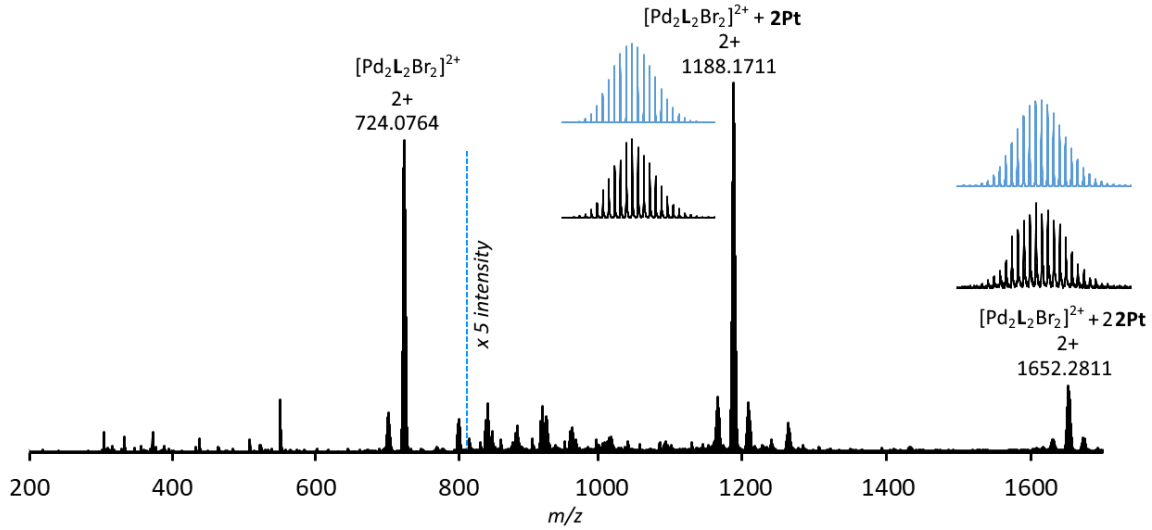

Figure 5.18 Partial mass spectrum (DMSO/acetonitrile, direct injection) of $[(\mathbf{2Pt})_2 \subset Pd_2\mathbf{L}_2Br_2]^{2+}$.

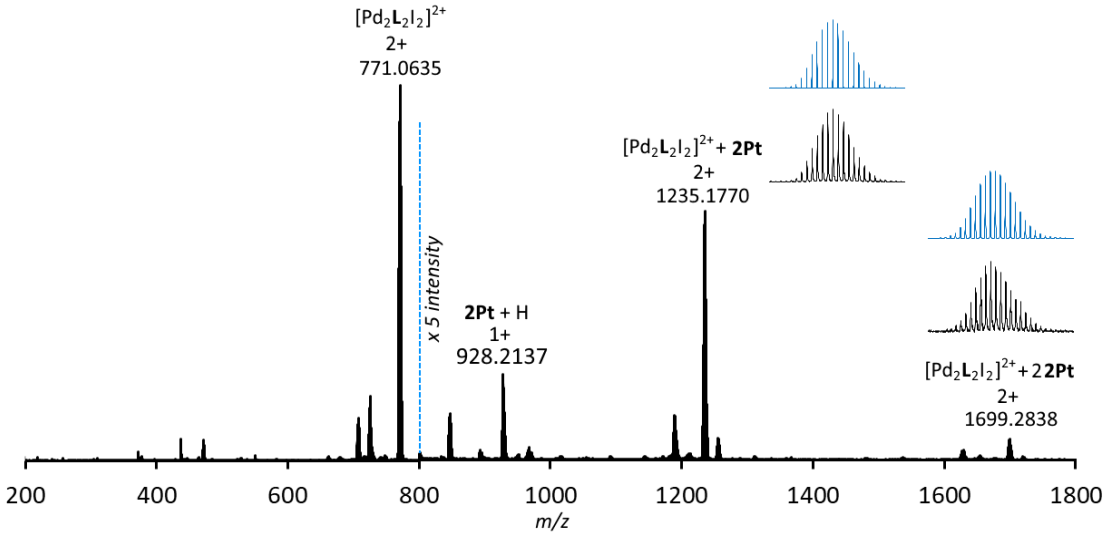

Figure 5.19 Partial mass spectrum (DMSO/acetonitrile, direct injection) of $[(\mathbf{2Pt})_2 \subset Pd_2\mathbf{L}_2I_2]^{2+}$.

5.4 Binding isotherms

The H_d triazole proton of the hosts was used to assess binding stoichiometry. This resonance was chosen because, across all hosts, it was the least prone to spectral crowding against other peaks, and hence the chemical shift could be accurately obtained. Using the mole ratio method,[19-20] the binding isotherms for all hosts with **2Pt** indicated 1:2 host/guest stoichiometry. We note that problems with the Job method and variants have been identified with 1:2 and higher binding stoichiometries.[20-21] The same works have identified that systems with 1:1 stoichiometries generally return accurate results. The 1:2 stoichiometries identified here do not definitively prove 1:2 adducts, but give strong evidence that the system is not 1:1.

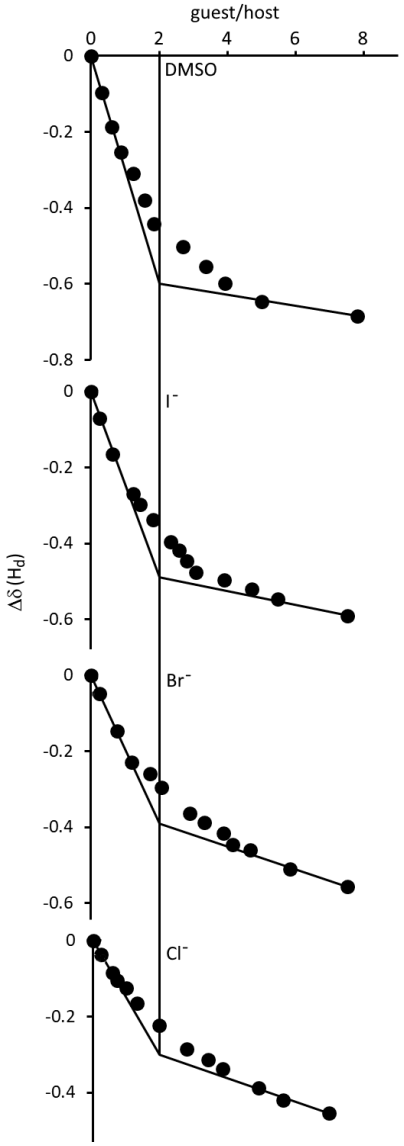

Figure 5.20 Changes in chemical shift of H_d for $[Pd_2\mathbf{L}_2\mathbf{L'}_2]^{n+}$ hosts (600 MHz, $[D_6]$DMSO, 298 K, 2.5 mM) upon introduction of **2Pt**. The identity of **L'** is given on the plot.

5.5 Calculation of binding constants and stoichiometries

Binding constants and stoichiometries were calculated[22-23] using the residual errors on the two proton resonances suitable for assessment across all systems during the titration experiments. The 1:2 full and additive methods were discarded for large percentage errors and/or nonsensical constants. Comparison of the 1:2 non-cooperative and statistical and 1:1 stoichiometries revealed that the 1:2 non-cooperative model had the lowest residual errors. This was also consistent with the mole ratio method (used to discount the 1:1 model), with support from mass spectrometry. We therefore find it most likely that **2Pt** binds in a 1:2 fashion host/guest ratio to the hosts in a manner best described as non-cooperative. We note that the ranking of binding constants is the same across non-cooperative, statistical, additive and 1:1 binding models.

5.5.1 L' = DMSO

Table 5.1 Observed and theoretical data with residual error for the two resonances able to be accurately assessed for chemical shift via ^{1}H NMR spectroscopy (600 MHz, [D_6]DMSO, 298 K), for the 1:1 model, for **L'** = DMSO.

Method: 1:1

EQ.	H_d observed	H_d theoretical	Residual error	H_l observed	H_l theoretical	Residual error
0.0	0.00	0.00	-	0.00	0.00	-
0.3	-0.10	-0.11	-0.0128	0.00	0.00	0.0001
0.6	-0.19	-0.19	0.0010	-0.01	-0.01	0.0009
0.9	-0.25	-0.26	-0.0026	-0.01	-0.01	0.0009
1.2	-0.31	-0.33	-0.0172	-0.02	-0.01	0.0009
1.6	-0.38	-0.38	-0.0025	-0.02	-0.02	0.0010
1.8	-0.44	-0.42	0.0217	-0.02	-0.02	0.0020
2.7	-0.50	-0.51	-0.0057	-0.02	-0.02	0.0004
3.4	-0.55	-0.56	-0.0043	-0.02	-0.02	0.0000
3.9	-0.60	-0.59	0.0090	-0.03	-0.03	0.0004
5.0	-0.65	-0.63	0.0141	-0.03	-0.03	-0.0006
8.0	-0.68	-0.70	-0.0138	-0.03	-0.03	-0.0027

Table 5.2 Root mean square (RMS) error and covariance for the ^{1}H NMR data (600 MHz, [D_6]DMSO, 298 K), for the 1:1 model, for **L'** = DMSO.

Method: 1:1

RMS: Proton 1	0.011053
RMS: Proton 2	0.001128
RMS: Total	0.007856
Covariance: Proton 1	0.002676
Covariance: Proton 2	0.015209
Covariance: Total	0.001082

Table 5.3 Observed and theoretical data with residual error for the two resonances able to be accurately assessed for chemical shift via ^{1}H NMR spectroscopy (600 MHz, [D_6]DMSO, 298 K), for the non-cooperative model, for **L'** = DMSO.

Method: Non-cooperative

EQ.	H_d observed	H_d theoretical	Residual error	H_l observed	H_l theoretical	Residual error
0.0	0.00	0.00	-	0.00	0.00	-
0.3	-0.10	-0.10	-0.0081	0.00	-0.01	-0.0004
0.6	-0.19	-0.18	0.0072	-0.01	-0.01	0.0001
0.9	-0.25	-0.25	0.0031	-0.01	-0.01	-0.0001
1.2	-0.31	-0.32	-0.0136	-0.02	-0.02	-0.0002
1.6	-0.38	-0.38	-0.0013	-0.02	-0.02	-0.0002
1.8	-0.44	-0.42	0.0207	-0.02	-0.02	0.0008
2.7	-0.50	-0.51	-0.0110	-0.02	-0.02	-0.0004
3.4	-0.55	-0.56	-0.0104	-0.02	-0.03	-0.0004
3.9	-0.60	-0.59	0.0036	-0.03	-0.03	0.0005
5.0	-0.65	-0.63	0.0119	-0.03	-0.03	0.0002
8.0	-0.68	-0.69	-0.0047	-0.03	-0.03	-0.0003

Table 5.4 Root mean square (RMS) error and covariance for the ^{1}H NMR data (600 MHz, [D_6]DMSO, 298 K), for the non-cooperative model, for **L'** = DMSO.

Method: Non-cooperative

RMS: Proton 1	0.009775
RMS: Proton 2	0.000368
RMS: Total	0.006917
Covariance: Proton 1	0.002112
Covariance: Proton 2	0.001697
Covariance: Total	0.00084

Table 5.5 Observed and theoretical data with residual error for the two resonances able to be accurately assessed for chemical shift via ^{1}H NMR spectroscopy (600 MHz, [D_6]DMSO, 298 K), for the statistical model, for **L'** = DMSO.

Method: Statistical

EQ.	H_d observed	H_d theoretical	Residual error	H_l observed	H_l theoretical	Residual error
0.0	0.00	0.00	-	0.00	0.00	-
0.3	-0.10	-0.09	0.0032	0.00	0.00	0.0008
0.6	-0.19	-0.17	0.0217	-0.01	-0.01	0.0018
0.9	-0.25	-0.24	0.0169	-0.01	-0.01	0.0017
1.2	-0.31	-0.31	-0.0046	-0.02	-0.01	0.0015
1.6	-0.38	-0.38	0.0020	-0.02	-0.02	0.0012
1.8	-0.44	-0.42	0.0195	-0.02	-0.02	0.0019
2.7	-0.50	-0.52	-0.0199	-0.02	-0.02	-0.0003
3.4	-0.55	-0.57	-0.0196	-0.02	-0.03	-0.0007
3.9	-0.60	-0.60	-0.0037	-0.03	-0.03	-0.0002
5.0	-0.65	-0.64	0.0094	-0.03	-0.03	-0.0008
8.0	-0.68	-0.68	0.0036	-0.03	-0.03	-0.0019

Table 5.6 Root mean square (RMS) error and covariance for the ^{1}H NMR data (600 MHz, [D_6]DMSO, 298 K), for the statistical model, for **L'** = DMSO.

Method: Statistical

RMS: Proton 1	0.013123
RMS: Proton 2	0.001257
RMS: Total	0.009322
Covariance: Proton 1	0.003684
Covariance: Proton 2	0.017754
Covariance: Total	0.001493

5.5.2 L' = I^-

Table 5.7 Observed and theoretical data with residual error for the two resonances able to be accurately assessed for chemical shift via ^{1}H NMR spectroscopy (600 MHz, [D_6]DMSO, 298 K), for the 1:1 model, for **L'** = I^-.

Method: 1:1

EQ.	H_d observed	H_d theoretical	Residual error	H_I observed	H_I theoretical	Residual error
0.00	0.00	0.00	-	0.00	0.00	-
0.26	-0.07	-0.07	-0.0034	0.02	0.02	-0.002
0.63	-0.17	-0.16	0.0040	0.05	0.05	-0.006
1.23	-0.27	-0.27	-0.0023	0.08	0.08	-0.006
1.43	-0.30	-0.30	-0.0046	0.09	0.08	-0.008
1.82	-0.34	-0.35	-0.0133	0.09	0.10	0.014
2.34	-0.40	-0.40	-0.0055	0.11	0.11	0.007
2.57	-0.42	-0.42	-0.0012	0.12	0.12	-0.006
2.81	-0.45	-0.44	0.0083	0.13	0.12	-0.007
3.08	-0.48	-0.46	0.0218	0.14	0.13	-0.008
3.90	-0.50	-0.50	-0.0004	0.14	0.14	-0.002
4.70	-0.52	-0.53	-0.0074	0.15	0.15	0.002
5.47	-0.55	-0.55	-0.0024	0.15	0.15	0.003
7.52	-0.59	-0.59	0.0014	0.16	0.17	0.009

Table 5.8 Root mean square (RMS) error and covariance for the ^{1}H NMR data (600 MHz, [D_6]DMSO, 298 K), for the 1:1 model, for **L'** = I^-.

Method: 1:1

RMS: Proton 1	0.007886
RMS: Proton 2	0.006636
RMS: Total	0.007288
Covariance: Proton 1	0.002059
Covariance: Proton 2	0.019306
Covariance: Total	0.00076

Table 5.9 Observed and theoretical data with residual error for the two resonances able to be accurately assessed for chemical shift via ^{1}H NMR spectroscopy (600 MHz, [D_6]DMSO, 298 K), for the non-cooperative model, for **L'** = I^-.

Method: Non-cooperative

EQ.	H_d observed	H_d theoretical	Residual error	H_I observed	H_I theoretical	Residual error
0.00	0.00	0.00	-	0.00	0.00	-
0.26	-0.07	-0.07	-0.0008	0.02	0.02	-0.0017
0.63	-0.17	-0.16	0.0086	0.05	0.05	-0.0050
1.23	-0.27	-0.27	0.0020	0.08	0.08	-0.0040
1.43	-0.30	-0.30	-0.0011	0.09	0.09	-0.0056
1.82	-0.34	-0.35	-0.0115	0.09	0.10	0.0164
2.34	-0.40	-0.40	-0.0059	0.11	0.12	0.0097
2.57	-0.42	-0.42	-0.0024	0.12	0.12	-0.0032
2.81	-0.45	-0.44	0.0064	0.13	0.13	-0.0045
3.08	-0.48	-0.46	0.0193	0.14	0.13	-0.0059
3.90	-0.50	-0.50	-0.0036	0.14	0.14	-0.0015
4.70	-0.52	-0.53	-0.0099	0.15	0.15	0.0003
5.47	-0.55	-0.55	-0.0035	0.15	0.15	-0.0003
7.52	-0.59	-0.58	0.0056	0.16	0.16	0.0013

Table 5.10 Root mean square (RMS) error and covariance for the ^{1}H NMR data (600 MHz, [D_6]DMSO, 298 K), for the non-cooperative model, for **L'** = I^-.

Method: Non-cooperative

RMS: Proton 1	0.007646
RMS: Proton 2	0.006015
RMS: Total	0.006879
Covariance: Proton 1	0.001938
Covariance: Proton 2	0.016065
Covariance: Total	0.000681

Table 5.11 Observed and theoretical data with residual error for the two resonances able to be accurately assessed for chemical shift via ^{1}H NMR spectroscopy (600 MHz, [D_6]DMSO, 298 K), for the statistical model, for **L'** = I^-.

Method: Statistical

EQ.	H_d observed	H_d theoretical	Residual error	H_I observed	H_I theoretical	Residual error
0.00	0.00	0.00	-	0.00	0.00	-
0.26	-0.07	-0.06	0.0081	0.02	0.02	-0.0056
0.63	-0.17	-0.14	0.0220	0.05	0.04	-0.0115
1.23	-0.27	-0.26	0.0112	0.08	0.07	-0.0101
1.43	-0.30	-0.29	0.0055	0.09	0.08	-0.0109
1.82	-0.34	-0.35	-0.0101	0.09	0.10	0.0127
2.34	-0.40	-0.41	-0.0095	0.11	0.11	0.0082
2.57	-0.42	-0.43	-0.0073	0.12	0.12	-0.0039
2.81	-0.45	-0.45	0.0008	0.13	0.13	-0.0046
3.08	-0.48	-0.46	0.0134	0.14	0.13	-0.0054
3.90	-0.50	-0.51	-0.0081	0.14	0.14	0.0002
4.70	-0.52	-0.53	-0.0116	0.15	0.15	0.0027
5.47	-0.55	-0.55	-0.0023	0.15	0.15	0.0027
7.52	-0.59	-0.58	0.0125	0.16	0.16	0.0056

Table 5.12 Root mean square (RMS) error and covariance for the ^{1}H NMR data (600 MHz, [D_6]DMSO, 298 K), for the statistical model, for **L'** = I^-.

Method: Statistical

RMS: Proton 1	0.010321
RMS: Proton 2	0.007201
RMS: Total	0.008899
Covariance: Proton 1	0.003431
Covariance: Proton 2	0.022182
Covariance: Total	0.00114

5.5.3 L' = Br^-

Table 5.13 Observed and theoretical data with residual error for the two resonances able to be accurately assessed for chemical shift via ^1H NMR spectroscopy (600 MHz, $[D_6]$DMSO, 298 K), for the 1:1 model, for **L'** = Br^-.

Method: 1:1

EQ.	H_d observed	H_d theoretical	Residual error	H_l observed	H_l theoretical	Residual error
0.00	0.00	0.00	-	0.00	0.00	-
0.26	-0.05	-0.05	-0.0038	0.02	0.02	0.0021
0.76	-0.15	-0.14	0.0071	0.05	0.05	0.0043
1.20	-0.23	-0.20	0.0267	0.08	0.08	-0.0036
1.72	-0.26	-0.27	-0.0063	0.10	0.10	-0.0020
2.06	-0.30	-0.30	-0.0036	0.12	0.11	-0.0029
2.89	-0.36	-0.37	-0.0049	0.14	0.14	0.0001
3.32	-0.39	-0.40	-0.0093	0.15	0.15	0.0009
3.89	-0.42	-0.43	-0.0126	0.16	0.16	0.0042
4.14	-0.45	-0.44	0.0059	0.17	0.17	-0.0021
4.67	-0.46	-0.46	-0.0038	0.18	0.18	-0.0030
5.82	-0.51	-0.51	0.0050	0.19	0.19	0.0017
7.52	-0.56	-0.55	0.0073	0.21	0.21	0.0013

Table 5.14 Root mean square (RMS) error and covariance for the ^1H NMR data (600 MHz, $[D_6]$DMSO, 298 K), for the 1:1 model, for **L'** = Br^-.

Method: 1:1

RMS: Proton 1	0.007886
RMS: Proton 2	0.006636
RMS: Total	0.007288
Covariance: Proton 1	0.002059
Covariance: Proton 2	0.019306
Covariance: Total	0.00076

Table 5.15 Observed and theoretical data with residual error for the two resonances able to be accurately assessed for chemical shift via ^{1}H NMR spectroscopy (600 MHz, [D_6]DMSO, 298 K), for the non-cooperative model, for **L'** = Br^-.

Method: Non-cooperative

EQ.	H_d observed	H_d theoretical	Residual error	H_l observed	H_l theoretical	Residual error
0.00	0.00	0.00	-	0.00	0.00	-
0.26	-0.05	-0.05	-0.0024	0.02	0.02	0.0019
0.76	-0.15	-0.14	0.0097	0.05	0.05	0.0041
1.20	-0.23	-0.20	0.0293	0.08	0.08	-0.0036
1.72	-0.26	-0.26	-0.0044	0.10	0.10	-0.0017
2.06	-0.30	-0.30	-0.0025	0.12	0.11	-0.0024
2.89	-0.36	-0.37	-0.0052	0.14	0.14	0.0009
3.32	-0.39	-0.40	-0.0102	0.15	0.15	0.0017
3.89	-0.42	-0.43	-0.0139	0.16	0.16	0.0049
4.14	-0.45	-0.44	0.0045	0.17	0.17	-0.0014
4.67	-0.46	-0.47	-0.0052	0.18	0.18	-0.0027
5.82	-0.51	-0.51	0.0044	0.19	0.19	0.0011
7.52	-0.56	-0.55	0.0091	0.21	0.21	-0.0010

Table 5.16 Root mean square (RMS) error and covariance for the ^{1}H NMR data (600 MHz, [D_6]DMSO, 298 K), for the non-cooperative model, for **L'** = Br^-.

Method: Non-cooperative

RMS: Proton 1	0.01059
RMS: Proton 2	0.0025
RMS: Total	0.007694
Covariance: Proton 1	0.003988
Covariance: Proton 2	0.001518
Covariance: Total	0.000922

Table 5.17 Observed and theoretical data with residual error for the two resonances able to be accurately assessed for chemical shift via ^{1}H NMR spectroscopy (600 MHz, [D_6]DMSO, 298 K), for the statistical model, for **L'** = Br^-.

Method: Statistical

EQ.	H_d observed	H_d theoretical	Residual error	H_l observed	H_l theoretical	Residual error
0.00	0.00	0.00	-	0.00	0.00	-
0.26	-0.07	-0.07	-0.0034	0.02	0.02	0.0005
0.76	-0.17	-0.16	0.0040	0.05	0.05	0.0015
1.20	-0.27	-0.27	-0.0023	0.08	0.08	-0.0061
1.72	-0.30	-0.30	-0.0046	0.09	0.08	-0.0036
2.06	-0.34	-0.35	-0.0133	0.09	0.10	-0.0037
2.89	-0.40	-0.40	-0.0055	0.11	0.11	0.0006
3.32	-0.42	-0.42	-0.0012	0.12	0.12	0.0019
3.89	-0.45	-0.44	0.0083	0.13	0.12	0.0054
4.14	-0.48	-0.46	0.0218	0.14	0.13	-0.0008
4.67	-0.50	-0.50	-0.0004	0.14	0.14	-0.0019
5.82	-0.52	-0.53	-0.0074	0.15	0.15	0.0020
7.52	-0.55	-0.55	-0.0024	0.15	0.15	-0.0001

Table 5.18 Root mean square (RMS) error and covariance for the ^{1}H NMR data (600 MHz, [D_6]DMSO, 298 K), for the statistical model, for **L'** = Br^-.

Method: Statistical

RMS: Proton 1	0.01059
RMS: Proton 2	0.0025
RMS: Total	0.007694
Covariance: Proton 1	0.003988
Covariance: Proton 2	0.001518
Covariance: Total	0.000922

5.5.4 L' = Cl^-

Table 5.19 Observed and theoretical data with residual error for the two resonances able to be accurately assessed for chemical shift via ^{1}H NMR spectroscopy (600 MHz, [D_6]DMSO, 298 K), for the 1:1 model, for **L'** = Cl^-.

Method: 1:1

EQ.	H_d observed	H_d theoretical	Residual error	H_l observed	H_l theoretical	Residual error
0.00	0.00	0.00	-	0.00	0.00	-
0.23	-0.04	-0.03	0.0034	0.01	0.01	0.0001
0.59	-0.08	-0.08	0.0027	0.02	0.02	-0.0020
0.73	-0.10	-0.10	0.0057	0.03	0.03	-0.0014
1.00	-0.13	-0.13	-0.0032	0.04	0.03	-0.0010
1.32	-0.16	-0.16	0.0025	0.05	0.04	-0.0050
2.00	-0.22	-0.22	-0.0003	0.07	0.06	-0.0075
2.82	-0.29	-0.28	0.0028	0.08	0.08	0.0004
3.46	-0.31	-0.32	-0.0060	0.08	0.09	0.0086
3.90	-0.34	-0.34	-0.0055	0.09	0.09	0.0057
5.00	-0.39	-0.39	-0.0015	0.11	0.11	-0.0005
5.74	-0.42	-0.42	0.0057	0.11	0.11	0.0024
7.12	-0.46	-0.45	0.0009	0.13	0.12	-0.0060

Table 5.20 Root mean square (RMS) error and covariance for the ^{1}H NMR data (600 MHz, [D_6]DMSO, 298 K), for the 1:1 model, for **L'** = Cl^-.

Method: 1:1

RMS: Proton 1	0.003692
RMS: Proton 2	0.004292
RMS: Total	0.004003
Covariance: Proton 1	0.000628
Covariance: Proton 2	0.011865
Covariance: Total	0.0005

Table 5.21 Observed and theoretical data with residual error for the two resonances able to be accurately assessed for chemical shift via ^{1}H NMR spectroscopy (600 MHz, [D_6]DMSO, 298 K), for the non-cooperative model, for **L'** = Cl^-.

Method: Non-cooperative

EQ.	H_d observed	H_d theoretical	Residual error	H_l observed	H_l theoretical	Residual error
0.00	0.00	0.00	-	0.00	0.00	-
0.23	-0.04	-0.03	0.0039	0.01	0.01	0.0000
0.59	-0.08	-0.08	0.0037	0.02	0.02	-0.0021
0.73	-0.10	-0.10	0.0067	0.03	0.03	-0.0015
1.00	-0.13	-0.13	-0.0022	0.04	0.03	-0.0011
1.32	-0.16	-0.16	0.0034	0.05	0.04	-0.0050
2.00	-0.22	-0.22	0.0000	0.07	0.06	-0.0074
2.82	-0.29	-0.28	0.0024	0.08	0.08	0.0007
3.46	-0.31	-0.32	-0.0067	0.08	0.09	0.0090
3.90	-0.34	-0.34	-0.0064	0.09	0.09	0.0060
5.00	-0.39	-0.39	-0.0022	0.11	0.11	-0.0004
5.74	-0.42	-0.42	0.0055	0.11	0.11	0.0023
7.12	-0.46	-0.45	0.0020	0.13	0.12	-0.0067

Table 5.22 Root mean square (RMS) error and covariance for the ^{1}H NMR data (600 MHz, [D_6]DMSO, 298 K), for the non-cooperative model, for **L'** = Cl^-.

Method: Non-cooperative

RMS: Proton 1	0.004104
RMS: Proton 2	0.004429
RMS: Total	0.004269
Covariance: Proton 1	0.000765
Covariance: Proton 2	0.012646
Covariance: Total	0.000568

Table 5.23 Observed and theoretical data with residual error for the two resonances able to be accurately assessed for chemical shift via ^{1}H NMR spectroscopy (600 MHz, [D_6]DMSO, 298 K), for the statistical model, for **L'** = Cl^-.

Method: Statistical

EQ.	H_d observed	H_d theoretical	Residual error	H_l observed	H_l theoretical	Residual error
0.00	0.00	0.00	-	0.00	0.00	-
0.26	-0.04	-0.03	0.0049	0.01	0.01	-0.0003
0.63	-0.08	-0.08	0.0053	0.02	0.02	-0.0027
1.23	-0.10	-0.10	0.0084	0.03	0.03	-0.0021
1.43	-0.13	-0.13	-0.0005	0.04	0.03	-0.0017
1.82	-0.16	-0.16	0.0047	0.05	0.04	-0.0056
2.34	-0.22	-0.22	0.0004	0.07	0.06	-0.0077
2.57	-0.29	-0.28	0.0017	0.08	0.08	0.0007
2.81	-0.31	-0.32	-0.0077	0.08	0.09	0.0091
3.08	-0.34	-0.34	-0.0074	0.09	0.09	0.0062
3.90	-0.39	-0.39	-0.0029	0.11	0.11	-0.0002
4.70	-0.42	-0.42	0.0053	0.11	0.11	0.0025
5.47	-0.46	-0.45	0.0030	0.13	0.12	-0.0066

Table 5.24 Root mean square (RMS) error and covariance for the ^{1}H NMR data (600 MHz, [D_6]DMSO, 298 K), for the statistical model, for **L'** = Cl^-.

Method: Statistical

RMS: Proton 1	0.004867
RMS: Proton 2	0.004629
RMS: Total	0.004749
Covariance: Proton 1	0.001053
Covariance: Proton 2	0.013698
Covariance: Total	0.000702

Table 5.25 Percentage errors for calculated binding constants.

	1:2 Binding between $[Pd_2L_2L'_2]^{n+}$ hosts and 2Pt						1:1 Binding
	Full		Non-cooperative	Statistical	Additive		
	K_{11} (M^{-1})	K_{12} (M^{-1})	K_{11} (M^{-1})	K_{11} (M^{-1})	K_{11} (M^{-1})	K_{12} (M^{-1})	K (M^{-1})
L' = DMSO	2.3%	2.3%	4.8%	7.7%	19.7%	10.7%	3.8%
L' = I^-	8.1%	34.1%	3.8%	6.4%	20.8%	10.9%	3.3%
L' = Br^-	(6.5×10^9)%	3.3%	3.8%	4.7%	7.6%	12.1%	2.9%
L' = Cl^-	11.0%	4.3%	2.4%	2.8%	4.7%	10.8%	1.9%

Table 5.26 Binding constants established from ^{1}H NMR spectroscopic titrations for **2Pt** with hosts in this study. Constants with errors higher than 35% shown in red, in italics for negative values. For non-cooperative and statistical models, only K_{11} is stated: K_{12} is one quarter of K_{11}

	1:2 Binding between $[Pd_2L_2L'_2]^{n+}$ hosts and 2Pt						1:1 Binding
	Full		Non-cooperative	Statistical	Additive		
	K_{11} (M^{-1})	K_{12} (M^{-1})	K_{11} (M^{-1})	K_{11} (M^{-1})	K_{11} (M^{-1})	K_{12} (M^{-1})	K (M^{-1})
L' = DMSO	225 ± 6	*-34 ± 1*	680 ± 30	1500 ± 200	1800 ± 400	220 ± 20	310 ± 20
L' = I^-	370 ± 30	70 ± 30	410 ± 20	1300 ± 100	1500 ± 400	170 ± 20	300 ± 10
L' = Br^-	$(4 \times 10^{17}) \pm (3 \times 10^{25})$	84 ± 3	250 ± 10	500 ± 30	330 ± 30	25 ± 4	159 ± 5
L' = Cl^-	800 ± 100	46 ± 2	179 ± 5	314 ± 9	200 ± 10	18 ± 2	108 ± 3

Table 5.27 Comparison of root mean square (RMS) error and co-variance between non-cooperative and statistical models. The higher errors are shown in red, the lowest in green.

	Non-cooperative (RMS) (Co-variance)	**Statistical (RMS) (Co-variance)**	**1:1 (RMS) (Co-variance)**
L' = DMSO	6.92×10^{-3} 8.40×10^{-4}	9.32×10^{-3} 1.49×10^{-3}	7.86×10^{-3} 1.08×10^{-3}
L' = I^-	6.88×10^{-3} 6.80×10^{-4}	8.90×10^{-3} 1.14×10^{-3}	7.29×10^{-3} 7.60×10^{-4}
L' = Br^-	7.69×10^{-3} 9.20×10^{-4}	8.92×10^{-3} 1.24×10^{-3}	7.10×10^{-3} 7.90×10^{-4}
L' = Cl^-	4.27×10^{-3} 5.70×10^{-4}	4.75×10^{-3} 7.00×10^{-4}	4.00×10^{-3} 5.00×10^{-4}
Average	6.44×10^{-3} 7.50×10^{-4}	7.97×10^{-3} 1.14×10^{-3}	6.56×10^{-3} 7.80×10^{-4}

6 References

1. Ouchi, M.; Inoue, Y.; Liu, Y.; Nagamune, S.; Nakamura, S.; Wada, K.; Hakushi, T., Convenient and efficient tosylation of oligoethylene glycols and the related alcohols in tetrahydrofuran-water in the presence of sodium hydroxide. *Bull. Chem. Soc. Jpn.* **1990,** *63* (4), 1260-2.
2. Allampally, N. K.; Bredol, M.; Strassert, C. A.; De Cola, L., Highly Phosphorescent Supramolecular Hydrogels Based on Platinum Emitters. *Chem. - Eur. J.* **2014,** *20* (51), 16863-16868.
3. Su, S.-J.; Tanaka, D.; Li, Y.-J.; Sasabe, H.; Takeda, T.; Kido, J., Novel Four-Pyridylbenzene-Armed Biphenyls as Electron-Transport Materials for Phosphorescent OLEDs. *Org. Lett.* **2008,** *10* (5), 941-944.
4. Motschi, H.; Nussbaumer, C.; Pregosin, P. S.; Bachechi, F.; Mura, P.; Zambonelli, L., Thetrans-Influence in Platinum (II) Complexes.1H- and13C-NMR. and X-ray structural studies of tridentateSchiff's base complexes of platinum (II). *Helv. Chim. Acta* **1980,** *63* (7), 2071-2086.
5. Neese, F., The ORCA program system. *WIREs Comput. Mol. Sci.* **2012,** *2* (1), 73-78.
6. Becke, A. D., Density-functional exchange-energy approximation with correct asymptotic behavior. *Phys. Rev. A: Gen. Phys.* **1988,** *38* (6), 3098-100.
7. Perdew, Density-functional approximation for the correlation energy of the inhomogeneous electron gas. *Phys. Rev. B: Condens. Matter* **1986,** *33* (12), 8822-8824.
8. Perdew; Yue, Accurate and simple density functional for the electronic exchange energy: Generalized gradient approximation. *Phys. Rev. B: Condens. Matter* **1986,** *33* (12), 8800-8802.
9. Schaefer, A.; Horn, H.; Ahlrichs, R., Fully optimized contracted Gaussian basis sets for atoms lithium to krypton. *J. Chem. Phys.* **1992,** *97* (4), 2571-7.
10. Neese, F., An improvement of the resolution of the identity approximation for the formation of the Coulomb matrix. *J. Comput. Chem.* **2003,** *24* (14), 1740-1747.
11. Eichkorn, K.; Treutler, O.; Oehm, H.; Haeser, M.; Ahlrichs, R., Auxiliary basis sets to approximate Coulomb potentials. *Chem. Phys. Lett.* **1995,** *240* (4), 283-90.
12. Eichkorn, K.; Treutler, O.; Oehm, H.; Haeser, M.; Ahlrichs, R., Auxiliary basis sets to approximate Coulomb potentials. [Erratum to document cited in CA123:93649]. *Chem. Phys. Lett.* **1995,** *242* (6), 652-60.
13. Eichkorn, K.; Weigend, F.; Treutler, O.; Ahlrichs, R., Auxiliary basis sets for main row atoms and transition metals and their use to approximate Coulomb potentials. *Theor. Chem. Acc.* **1997,** *97* (1-4), 119-124.
14. Schweinfurth, D.; Pattacini, R.; Strobel, S.; Sarkar, B., New 1,2,3-triazole ligands through click reactions and their palladium and platinum complexes. *Dalton Trans.* **2009,** (42), 9291-9297.
15. Schweinfurth, D.; Strobel, S.; Sarkar, B., Expanding the scope of Click derived 1,2,3-triazole ligands: New palladium and platinum complexes. *Inorg. Chim. Acta* **2011,** *374* (1), 253-260.
16. Jindabot, S.; Teerachanan, K.; Thongkam, P.; Kiatisevi, S.; Khamnaen, T.; Phiriyawirut, P.; Charoenchaidet, S.; Sooksimuang, T.; Kongsaeree, P.; Sangtrirutnugul, P., Palladium(II) complexes featuring bidentate pyridine-triazole ligands: Synthesis, structures, and catalytic activities for Suzuki-Miyaura coupling reactions. *J. Organomet. Chem.* **2014,** *750*, 35-40.
17. Joseph, M. C.; Swarts, A. J.; Mapolie, S. F., Palladium (II) complexes chelated by 1-substituted-4-pyridyl-1H-1,2,3-triazole ligands as catalyst precursors for selective ethylene dimerization. *Appl. Organomet. Chem.* **2020,** *34* (5), e5595.
18. Lo, W. K.; Huff, G. S.; Cubanski, J. R.; Kennedy, A. D.; McAdam, C. J.; McMorran, D. A.; Gordon, K. C.; Crowley, J. D., Comparison of inverse and regular 2-pyridyl-1,2,3-triazole "click" complexes: structures, stability, electrochemical, and photophysical properties. *Inorg. Chem.* **2015,** *54* (4), 1572-87.

19. Meyer, A. S.; Ayres, G. H., The Mole Ratio Method for Spectrophotometric Determination of Complexes in Solution. *J. Am. Chem. Soc.* **1957,** *79* (1), 49-53.
20. Brynn Hibbert, D.; Thordarson, P., The death of the Job plot, transparency, open science and online tools, uncertainty estimation methods and other developments in supramolecular chemistry data analysis. *Chem. Commun.* **2016,** *52* (87), 12792-12805.
21. Ulatowski, F.; Dąbrowa, K.; Bałakier, T.; Jurczak, J., Recognizing the Limited Applicability of Job Plots in Studying Host–Guest Interactions in Supramolecular Chemistry. *J. Org. Chem.* **2016,** *81* (5), 1746-1756.
22. Thordarson, P., Determining association constants from titration experiments in supramolecular chemistry. *Chem. Soc. Rev.* **2011,** *40* (3), 1305-1323.
23. www.supramolecular.org.